



## Calhoun: The NPS Institutional Archive

---

Theses and Dissertations

Thesis Collection

---

2011-09

# Adaptive control and parameter identification of a doubly-fed induction generator for wind power

Orfanos-Pepainas, Stamatios

Monterey, California. Naval Postgraduate School

---

<http://hdl.handle.net/10945/5510>



Calhoun is a project of the Dudley Knox Library at NPS, furthering the precepts and goals of open government and government transparency. All information contained herein has been approved for release by the NPS Public Affairs Officer.

**Dudley Knox Library / Naval Postgraduate School**  
**411 Dyer Road / 1 University Circle**  
**Monterey, California USA 93943**

<http://www.nps.edu/library>



# **NAVAL POSTGRADUATE SCHOOL**

**MONTEREY, CALIFORNIA**

## **THESIS**

**ADAPTIVE CONTROL AND PARAMETER  
IDENTIFICATION OF A DOUBLY-FED INDUCTION  
GENERATOR FOR WIND POWER**

by

Stamatios Orfanos - Pepainas

September 2011

Thesis Co-Advisors:

Roberto Cristi  
Alexander L. Julian  
Xiaoping Yun

Second Reader:

**Approved for public Release; distribution is unlimited**

THIS PAGE INTENTIONALLY LEFT BLANK

<b>REPORT DOCUMENTATION PAGE</b>			<i>Form Approved OMB No. 0704-0188</i>	
Public reporting burden for this collection of information is estimated to average 1 hour per response, including the time for reviewing instruction, searching existing data sources, gathering and maintaining the data needed, and completing and reviewing the collection of information. Send comments regarding this burden estimate or any other aspect of this collection of information, including suggestions for reducing this burden, to Washington headquarters Services, Directorate for Information Operations and Reports, 1215 Jefferson Davis Highway, Suite 1204, Arlington, VA 22202-4302, and to the Office of Management and Budget, Paperwork Reduction Project (0704-0188) Washington DC 20503.				
<b>1. AGENCY USE ONLY (Leave blank)</b>		<b>2. REPORT DATE</b> September 2011	<b>3. REPORT TYPE AND DATES COVERED</b> Master's Thesis	
<b>4. TITLE AND SUBTITLE</b> Adaptive Control and Parameter Identification of a Doubly-Fed Induction Generator for Wind Power			<b>5. FUNDING NUMBERS</b>	
<b>6. AUTHOR(S)</b> Stamatios Orfanos-Pepainas				
<b>7. PERFORMING ORGANIZATION NAME(S) AND ADDRESS(ES)</b> Naval Postgraduate School Monterey, CA 93943-5000			<b>8. PERFORMING ORGANIZATION REPORT NUMBER</b>	
<b>9. SPONSORING /MONITORING AGENCY NAME(S) AND ADDRESS(ES)</b> N/A			<b>10. SPONSORING/MONITORING AGENCY REPORT NUMBER</b>	
<b>11. SUPPLEMENTARY NOTES</b> The views expressed in this thesis are those of the author and do not reflect the official policy or position of the Department of Defense or the U.S. Government. IRB Protocol number: N/A.				
<b>12a. DISTRIBUTION / AVAILABILITY STATEMENT</b> 1. Approved for public release; distribution unlimited			<b>12b. DISTRIBUTION CODE</b>	
<b>13. ABSTRACT (maximum 200 words)</b>  The use of Doubly-Fed Induction Generators (DFIG) for wind energy conversion is addressed in this thesis. It is well known that when the stator is connected to the electric grid, the rotor voltage can control both mechanical torque and reactive electric power. To guarantee efficient wind energy conversion, it is important to research and design more advanced control schemes. In this thesis, we first review the basic theory behind DFIGs and Adaptive Control. Next we design an adaptive controller for a wind turbine using a DFIG and model and simulate the system. In order to create a valid assessment on the results of this method, we compare the system's performance with a standard control scheme based on proportional integral (PI) controllers as proposed in standard approaches.				
<b>14. SUBJECT TERMS</b> Wind Energy, DFIG, Adaptive Control			<b>15. NUMBER OF PAGES</b> 103	
			<b>16. PRICE CODE</b>	
<b>17. SECURITY CLASSIFICATION OF REPORT</b> Unclassified	<b>18. SECURITY CLASSIFICATION OF THIS PAGE</b> Unclassified	<b>19. SECURITY CLASSIFICATION OF ABSTRACT</b> Unclassified	<b>20. LIMITATION OF ABSTRACT</b> UU	

NSN 7540-01-280-5500

Standard Form 298 (Rev. 8-98)  
Prescribed by ANSI Std. Z39.18

THIS PAGE INTENTIONALLY LEFT BLANK

**Approved for public release; distribution is unlimited**

**ADAPTIVE CONTROL AND PARAMETER IDENTIFICATION OF A DOUBLY-  
FED INDUCTION GENERATOR FOR WIND POWER**

Stamatios Orfanos-Pepainas  
Lieutenant, Hellenic Navy  
BS, Hellenic Naval Academy, June 2001

Submitted in partial fulfillment of the  
requirements for the degrees of

**ELECTRICAL ENGINEER**  
and  
**MASTER OF SCIENCE IN ELECTRICAL ENGINEERING**

from the

**NAVAL POSTGRADUATE SCHOOL**  
**September 2011**

Author: Stamatios Orfanos-Pepainas

Approved by: Roberto Cristi  
Thesis Co-Advisor

Alexander L. Julian  
Thesis Co-Advisor

Xiaoping Yun  
Second Reader

R. Clark Robertson  
Chair, Department of Electrical and Computer Engineering

THIS PAGE INTENTIONALLY LEFT BLANK

## **ABSTRACT**

The use of Doubly-Fed Induction Generators (DFIG) for wind energy conversion is addressed in this thesis. It is well known that when the stator is connected to the electric grid, the rotor voltage can control both mechanical torque and reactive electric power.

To guarantee efficient wind energy conversion, it is important to research and design more advanced control schemes. In this thesis, we first review the basic theory behind DFIGs and Adaptive Control. Next we design an adaptive controller for a wind turbine using a DFIG and model and simulate the system. In order to create a valid assessment on the results of this method, we compare the system's performance with a standard control scheme based on proportional integral (PI) controllers as proposed in standard approaches.



THIS PAGE INTENTIONALLY LEFT BLANK

# TABLE OF CONTENTS

<b>I.</b>	<b>INTRODUCTION.....</b>	<b>1</b>
A.	<b>BACKGROUND .....</b>	<b>1</b>
B.	<b>THESIS OBJECTIVES.....</b>	<b>2</b>
C.	<b>RELATED WORK .....</b>	<b>2</b>
D.	<b>APPROACH.....</b>	<b>4</b>
E.	<b>THESIS OUTLINE.....</b>	<b>4</b>
A.	<b>WIND TURBINE THEORY.....</b>	<b>4</b>
1.	<b>Energy in the Wind.....</b>	<b>5</b>
2.	<b>Wind Turbine Aerodynamics – Disc Actuator Model.....</b>	<b>6</b>
3.	<b>Torque and Power on the Rotor .....</b>	<b>10</b>
4.	<b>Regions of Control .....</b>	<b>13</b>
B.	<b>DOUBLY-FED INDUCTION GENERATOR (DFIG) .....</b>	<b>14</b>
1.	<b>Reference Frames – Dynamic Models.....</b>	<b>15</b>
2.	<b>DFIG Model.....</b>	<b>18</b>
C.	<b>CHAPTER SUMMARY.....</b>	<b>19</b>
<b>III.</b>	<b>ONLINE PARAMETER ESTIMATION .....</b>	<b>21</b>
A.	<b>INTRODUCTION.....</b>	<b>21</b>
B.	<b>SYSTEM EQUATIONS .....</b>	<b>22</b>
C.	<b>ESTIMATORS.....</b>	<b>23</b>
1.	<b>Least Mean Squares (LMS) .....</b>	<b>23</b>
a.	<i>Equations Setup .....</i>	<i>24</i>
b.	<i>Implementation .....</i>	<i>26</i>
2.	<b>Recursive Least Squares (RLS) .....</b>	<b>28</b>
a.	<i>Equations Setup .....</i>	<i>28</i>
b.	<i>Implementation .....</i>	<i>29</i>
3.	<b>RLS With Exponential Forgetting (RLS-EF).....</b>	<b>30</b>
a.	<i>Equations Setup .....</i>	<i>30</i>
b.	<i>Implementation .....</i>	<i>31</i>
D.	<b>SIMULATION OF THE ESTIMATORS.....</b>	<b>31</b>
1.	<b>Equipment .....</b>	<b>31</b>
2.	<b>Simulation Results .....</b>	<b>32</b>
a.	<i>Simulation Using LMS .....</i>	<i>32</i>
b.	<i>Simulation Using RLS .....</i>	<i>34</i>
E.	<b>CHAPTER SUMMARY.....</b>	<b>36</b>
<b>IV.</b>	<b>ADAPTIVE CONTROL .....</b>	<b>39</b>
A.	<b>INTRODUCTION.....</b>	<b>39</b>
B.	<b>ADAPTIVE CONTROL THEORY .....</b>	<b>40</b>
C.	<b>ADAPTIVE CONTROL OF DFIG.....</b>	<b>41</b>
1.	<b>First Approach: Adaptive Control for Torque and Reactive Power.....</b>	<b>41</b>
a.	<i>Dynamic Model .....</i>	<i>41</i>

	<i>b.</i>	<i>Simulation Model</i> .....	48
	<i>c.</i>	<i>Simulation Results</i> .....	52
2.		Second Approach: Adaptive Control of Torque, PI Control of the Reactive Power.....	55
	<i>a.</i>	<i>Dynamic Model of the Controller</i> .....	55
	<i>b.</i>	<i>Simulation Model</i> .....	57
	<i>c.</i>	<i>Simulation Results</i> .....	58
3.		Performance Comparison .....	62
D.		CHAPTER SUMMARY .....	66
V.		CONCLUSIONS AND RECOMMENDATIONS.....	67
A.		SUMMARY - CONCLUSIONS.....	67
B.		RECOMMENDATIONS-FUTURE RESEARCH.....	68
APPENDIX:		MATLAB CODES - SIMULINK MODEL .....	69
A.		MATLAB CODE FOR INITIALIZATION OF THE SIMULATIONS ..	69
B.		SIMULINK BLOCKS .....	71
	1.	First Adaptive Control Approach .....	71
		<i>a.</i> <i>Overall System View</i> .....	71
		<i>b.</i> <i>Aerodynamic Torque Input</i> .....	72
		<i>c.</i> <i>General View of the Controller</i> .....	72
		<i>d.</i> <i>Preprocess</i> .....	73
		<i>e.</i> <i>Parameter Estimation</i> .....	73
		<i>f.</i> <i>Control</i> .....	74
	2.	Second Approach .....	74
		<i>a.</i> <i>Preprocess</i> .....	74
		<i>b.</i> <i>Control</i> .....	75
		LIST OF REFERENCES.....	77
		INITIAL DISTRIBUTION LIST .....	81

## LIST OF FIGURES

Figure 1.	Global wind power installations, 1996 to 2010. From [1].	1
Figure 2.	A volume of air flowing with speed $V$ .	5
Figure 3.	Actuator disc. After [14].	7
Figure 4.	Pressure around actuator disk. After [15].	8
Figure 5.	Turbine disc.	11
Figure 6.	Typical $C_p$ versus speed ratio $\lambda$ curve.	12
Figure 7.	Example power curves for a typical commercial WT. From [5].	13
Figure 8.	Induction machine cross section. From [20].	15
Figure 9.	General view of the DFIG model.	18
Figure 10.	General view of the LMS estimation model.	26
Figure 11.	Detailed block diagram for the LMS estimator model.	27
Figure 12.	General view of RLS estimator model.	29
Figure 13.	Detailed view of RLS estimator model.	30
Figure 14.	Convergence of $r_s$ and $r_r'$ using LMS from simulation.	33
Figure 15.	Convergence of $L_m$ using LMS from simulation.	33
Figure 16.	Convergence of $L_{ls}$ and $L_{lr}'$ using LMS from simulation.	34
Figure 17.	Convergence of $r_s$ and $r_r'$ using RLS from simulation.	35
Figure 18.	Convergence of $L_m$ using RLS from simulation.	35
Figure 19.	Convergence of $L_{ls}$ and $L_{lr}'$ using RLS from simulation.	36
Figure 20.	Direct MRAC overview. After [31].	40
Figure 21.	General view of the first controller in Simulink.	48
Figure 22.	Control block for the first approach.	49
Figure 23.	Wind speed and torque during simulation of the first approach.	53
Figure 24.	Magnified torque plot during simulation of the first approach.	53
Figure 25.	Real power ( $P_e$ ) during simulation of the first approach.	54
Figure 26.	Reactive power ( $Q_e$ ) during simulation of the first approach.	54
Figure 27.	Comparison of the rotor currents $i_{qr}$ and $i_{dr}$ with their reference values during simulation of the first approach.	55
Figure 28.	General view of the second controller model.	57
Figure 29.	Control block for the second approach.	58
Figure 30.	Wind speed and torque during simulation of the second approach.	59
Figure 31.	Magnified torque during simulation of the second approach.	60
Figure 32.	Real power ( $P_e$ ) during simulation of the second approach.	60
Figure 33.	Reactive power ( $Q_e$ ) during simulation of the second approach.	61
Figure 34.	Comparison between real and reactive power $P_e$ and $Q_e$ , respectively, for part of the simulation during the second approach.	61
Figure 35.	Comparison of the currents $i_{qs}$ and $i_{dr}$ with their reference values during simulation of the second approach.	62
Figure 36.	Wind profile for comparison of the control approaches.	63
Figure 37.	Comparison of output torque $T_e$ and reference torque $T_{ref}$ during the simulation of a wind gust.	63

Figure 38.	Magnified plot of output torque $T_e$ and reference torque $T_{ref}$ during the simulation of a wind gust.....	64
Figure 39.	Typical DFIG torque versus time curve for different values of $r_r$ .....	65
Figure 40.	Comparison of the variation of the output torque curves during simulation of a variation of $r_r$ .....	65
Figure 41.	Comparison of the variation of the DFIG speed during the simulation of a variation of $r_r$ .....	66

## LIST OF TABLES

Table 1.	Adaptation gains for the LMS simulation.....	28
Table 2.	Measured DFIG parameters. From [28].....	32
Table 3.	WT and DFIG parameters. From [7]. ....	51
Table 4.	Final simulation parameter values for first approach. ....	52
Table 5.	Final simulation parameter values for the second approach.....	59

THIS PAGE INTENTIONALLY LEFT BLANK

## LIST OF ACRONYMS AND ABBREVIATIONS

AC	Alternating Current
COE	Cost of Energy
$C_p$	Power coefficient of the Wind Turbine
$C_q$	Torque coefficient of the Wind Turbine
DFIG	Doubly Fed Induction Generator
DMRAC	Direct Model Reference Adaptive Control
$E_k$	Kinetic Energy
$F_D$	Force that is applied from the air flow on the actuator disc
HAWT	Horizontal Axis Wind Turbine
$i_{qd0r}$	Rotor currents in the arbitrary dq0 reference frame
$i_{qd0s}$	Stator currents in the arbitrary dq0 reference frame
J	Combined rotor and wind turbine inertia coefficient
$L_{lr}$	Leakage inductance of rotor winding
$L_{ls}$	Leakage inductance of stator winding
MIMO	Multi Input Multi Output
MMF	Magneto Motive Force
MRAC	Model Reference Adaptive Control
p	differential operator d/dt
P	The Number of poles of the generator
$P_D$	Power extracted from the wind by the actuator disc
PDF	Probability Density Function
$P_{er}$	Rotor Real power output
$P_{es}$	Stator Real power output
PI	Proportional Integral
$P_v$	Power in the Wind
PWM	Pulse Width Modulation
$Q_{er}$	Rotor Reactive power output
$Q_{es}$	Stator Reactive power output
R	Wind Turbine Blade radius
RE	Renewable Energy



$r_r$	Rotor resistance of the generator per phase.
$r_s$	Stator resistance of the generator per phase.
$s$	The Laplacian Operator
SM	Sliding Mode
$T_e$	Electromagnetic Torque output by the Generator
$T_r$	Aerodynamic Torque produced by the Wind Turbine
$T_{ref}$	Controller Reference Torque
$V$	Wind speed in m/s
$V_{qd0r}$	Rotor voltages in the arbitrary dq0 reference frame
$V_{qd0s}$	Stator voltages in the arbitrary dq0 reference frame
WE	Wind Energy
WECS	Wind Energy Conversion System
WT	Wind Turbine
$\lambda$	Tip speed to wind speed ratio of the Wind Turbine
$\lambda_{opt}$	Tip speed to wind speed ratio of the Wind Turbine for maximum power
$\lambda_{qd0r}$	Rotor flux linkages in dq0 reference frame
$\lambda_{qd0s}$	Stator flux linkages in dq0 reference frame
$\omega_r$	Rotational speed of rotor
$\Omega_r$	Wind turbine Rotational speed in rads/s

## EXECUTIVE SUMMARY

The possibility of fossil fuel shortages in the near future and environmental concerns about power generation has lead to an increasing demand for renewable energy (RE) installations worldwide. Among them, wind energy (WE) is one of the fastest growing. This form of energy production is suitable for electricity production since wind is available everywhere. However, the random nature of the wind and the need to provide a stable source for the grid calls for the design of effective control systems for wind energy conversion systems (WECS). This would improve both the reliability of the energy captured and the overall efficiency of the system.

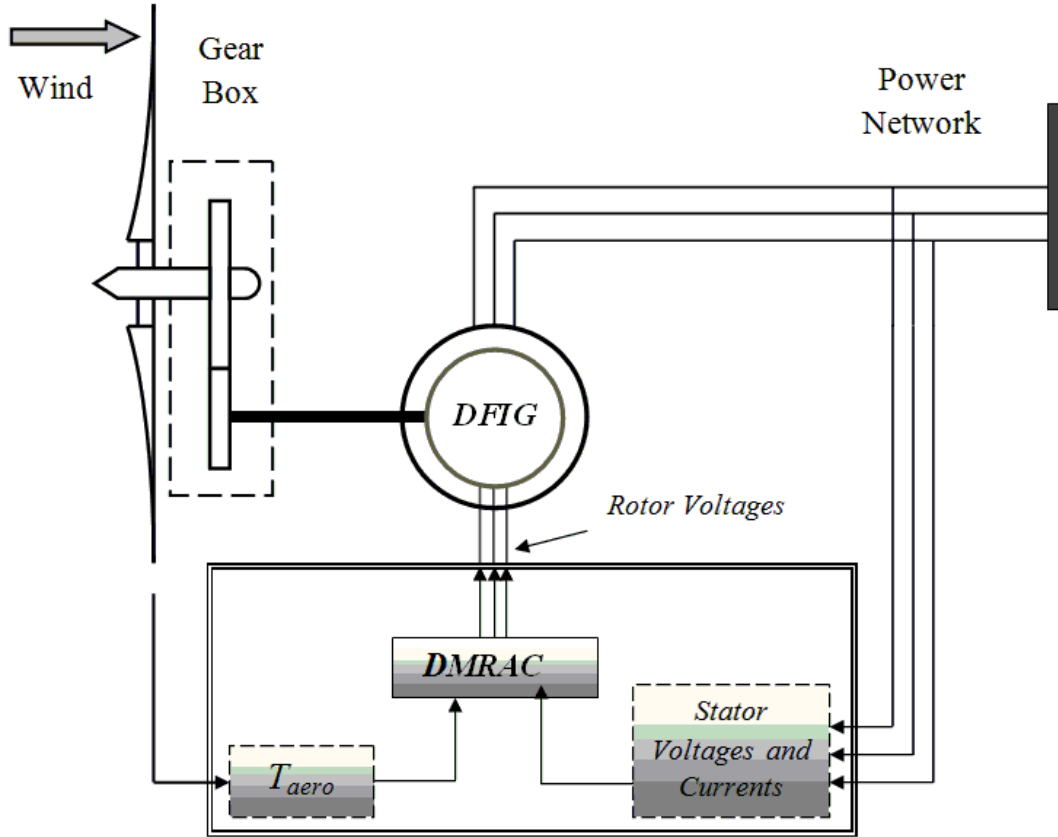
Many large wind power generators today are based on the doubly-fed induction generator (DFIG). The DFIG is capable of controlling both the active and reactive power simultaneously and keeping the generator at its maximum efficiency, even in the presence of wind speed variations. To take advantage of these features, the DFIG requires proper control in terms of its power electronics and computer algorithms.

Standard controllers, such as proportional integral (PI) controllers for pulse width modulation (PWM) converters at the rotor and source side of the system are the most commonly used to provide independent control of active and reactive power output.

A different control approach based on adaptive control theory is investigated in this thesis. The motivation for this research is the fact that WECS operate in environments with extreme variations in the operating conditions, and their operation depends on the wind speed, which, in general is a random process that cannot be controlled. Adaptive control systems, on the other hand, have the ability to “adapt” to variations in the system’s parameters, which is a very attractive feature. Among the various kinds of adaptive control methods, the one examined in this thesis is direct model reference adaptive control (DMRAC). The basic idea behind this approach is to make the system behave as closely as possible to a reference model in the presence of uncertain and/or time-varying dynamics of the system to be controlled. To achieve this, the system is modeled in terms of a vector of parameters  $\theta_c(t)$  that may be known or approximately

known. This parameter vector is updated by an adaptive law using input and output data. The goal of the controller is to continuously estimate the parameters creating a vector  $\hat{\theta}_c(t)$  to drive the error of the output vector  $\tilde{z}(t)$  between the reference model and the actual plant to zero.

A number of methods for system modeling and parameter identification, in terms of effectiveness and complexity, are investigated in this thesis. To improve the system's overall performance and stability under various operating conditions and faults, the results of the parameter identification are applied to the design of an adaptive controller for a power grid connected WECS. A basic view of the overall system is illustrated in the following figure.



General view of the proposed WECS.

Since there are two independent control channels, one for the active and one for the reactive power, and they both have different requirements, the effectiveness of using either two independent adaptive controllers or a combination of one adaptive and one classical PI controller is considered. One can reason that the reactive power has simple control requirements since it has to be kept to a constant value. The active power, on the other hand, has to follow a profile for maximum torque, which changes with wind velocity and the aerodynamics of the turbine.

To test and assess the effectiveness of the proposed techniques and their ability to adapt to changes in dynamics, a number of different cases have been simulated, such as changes in internal resistances and wind gusts.

It was found that DMRAC can be effectively applied in a WECS, which can significantly improve the performance of the overall system. To that end, a physical implementation to validate the results of this thesis is recommended.

THIS PAGE INTENTIONALLY LEFT BLANK

## **ACKNOWLEDGMENTS**

First, I would like to express my gratitude to my parents, Dimitrio and Eleni for teaching me the importance of education and for all the sacrifices they made to raise me and teach me all their principles in life.

I would like to thank my thesis advisor, Professor Roberto Cristi, for his continuous support and motivation not only throughout my research, but through the whole period of my studies here in NPS. I would also like to thank professors Xiaoping Yun and Alexander Julian, for their advice and the expansive knowledge that they passed on to me during my pursuit of graduate education.

I dedicate this work to my wife, Lina, and my daughter Danae, who have always been patient and supportive and provide me with the courage and inspiration needed to achieve my goals in life.

THIS PAGE INTENTIONALLY LEFT BLANK

# I. INTRODUCTION

## A. BACKGROUND

The possibility of a shortage in fossil fuels in the near future in conjunction with the continuously increasing demand for energy [1], [2] and environmental concerns about high emissions has contributed to a high interest in renewable energy (RE) worldwide. Among the various sources of RE, one of the fastest growing and most promising is wind power. New wind power capacity added globally during 2010 reached 39 GW, which is more than any other renewable technology and over three times higher than the 11.5 GW of wind power added worldwide in 2005. As a result, existing capacity increased more than 24% relative to 2009, with total global capacity close to 198 GW by the end of 2010 [3]. The growth of the global wind power installations over the past 15 years is demonstrated in Figure 1.

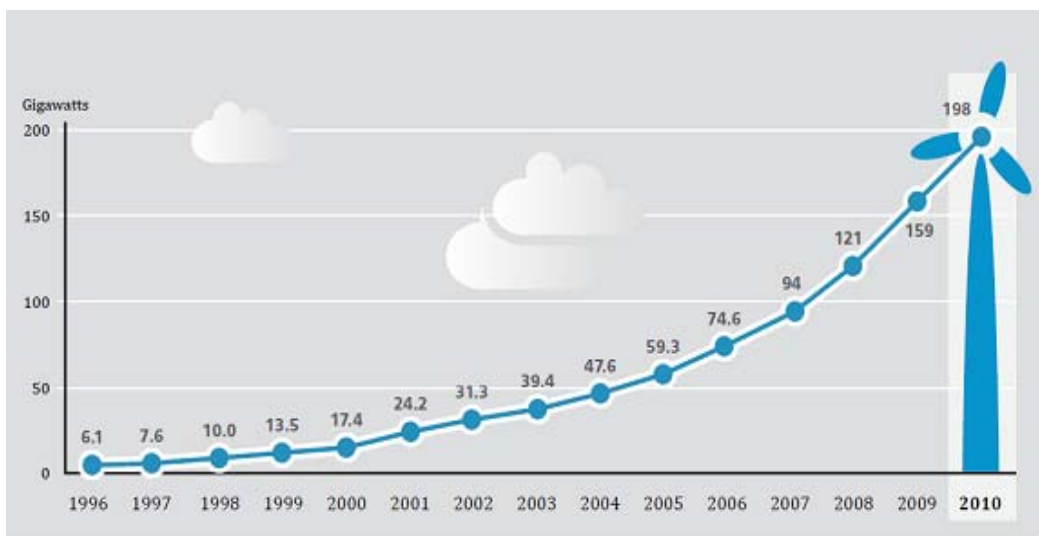


Figure 1. Global wind power installations, 1996 to 2010. From [1].



In the U.S., the wind industry started to grow in the 1980s; by 1986, the installed capacity in California was close to 90% of the global installed wind power. It later hit a plateau during an electricity restructuring period in the 1990s and regained momentum in the past decade [4].

The spread of wind energy (WE) installations indicates the need to develop wind turbines (WT) with higher efficiency. This involves technology advances that reduce the initial cost of the WT or allow the capture of more energy during operation, which results in a cost-of-energy (COE) decrease [5]. One approach that can lead to more effective WT is the design of more sophisticated controllers. The problem of designing an adaptive controller for a variable speed horizontal axis WT (HAWT) using a doubly-fed induction generator (DFIG) is addressed in this thesis.

## **B. THESIS OBJECTIVES**

The objective of this thesis is to apply various methods of system identification to a DFIG and investigate the design of an adaptive controller for a power grid connected wind energy conversion system (WECS) to improve the system's overall performance and stability under various operating conditions and faults. To achieve those goals, attempts are made to control both mechanical torque and reactive electric power independently using the rotor voltage components as a control input.

## **C. RELATED WORK**

Various researchers over the past several years have addressed the problem of efficient control of WECSs. The complexity of the overall system and the random conditions under which WTs operate have led scientists to investigate different control approaches to improve performance and stability under various fault conditions. A novel control method for smoothing the stator active or reactive power ripple components under unbalanced grid voltage is proposed in [6]. In [7], the design of a multi-input multi-output (MIMO) sliding mode (SM) nonlinear control strategy for a WECS is presented. The resulting robust control law guarantees finite time convergence, whereas smoothing discontinuities at the basis of sliding mode control achieves chattering reduction. The

paper concludes that this type of control is a particularly suitable option to deal with electronically controlled variable speed operating WECS. Furthermore, SM control has proven to be robust with respect to system parameter variations and external disturbances as well as poorly known operating environments [8], [9]. In [10], direct model reference adaptive control (DMRAC) was used to design an adaptive collective pitch controller for a HAWT. The objective of the adaptive pitch controller was to regulate generator speed for wind speeds higher than the rated value for the generator and to reject step disturbances. This objective was accomplished by collectively pitching the turbine blades. The results were compared in simulations with a classical proportional integrator (PI) collective pitch controller. In the simulations, the adaptive pitch controller showed better speed regulation for high wind speeds.

A different approach of optimal adaptive control is presented in [11] for a permanent magnet synchronous generator driven by a pulse width modulation (PWM) inverter. The controller focused on optimization of the system by minimizing Joule losses in the inverter and generator. To achieve this, the paper proposed the operation of the system at an operating point with minimum phase current, considering fixed torque.

Other, more classical approaches include the independent control of active and reactive power using back-to-back PWM voltage source converters in the rotor circuit. A vector control scheme on the supply side PWM ensures independent control of active and reactive power drawn from the supply, while vector control of the rotor side PWM results in a wide speed - range operation. The control is achieved using PI controllers to enable maximum speed tracking for maximum power extraction from the wind. This approach, presented in [12], presents two different controls, a current-mode control and a speed-mode control. A similar approach was presented in [13], where a Stator-Flux Oriented vector control approach is deployed for both stator and rotor side converters to provide independent control of active and reactive power using a decoupled design based on internal model control.

## **D. APPROACH**

In the first part of this research, the analytical design of an online identification algorithm is presented, with the intent of constructing a Simulink model of the physical system. In the second part, an adaptive control scheme to compensate for dynamic variations of the generator is proposed and its effectiveness is evaluated by computer simulations. In the simulations, various fault conditions are implemented, and the results are discussed subsequently.

## **E. THESIS OUTLINE**

This thesis is organized as follows: the concept of the basic theory of WTs and DFIGs is covered in Chapter II, and the model created for the system in the Simulink environment is described. The theory of online system identification including modeling and simulation results for different estimation algorithms, is covered in Chapter III. A basic introduction to adaptive control theory and the design and simulation of two different adaptive controllers, along with simulation results under different operational conditions of the system, are presented in Chapter IV. A comparison with simulation results from other control approaches is also presented. Finally, the conclusions based on the results from the previous chapters, along with some recommendations for future research in the area of adaptive control for WTs, are presented in Chapter V. The Appendix includes Matlab code for initialization of the simulation of the controllers as well as the basic model blocks in the Simulink environment.

II. WIND TURBINES – DFIG

## **A. WIND TURBINE THEORY**

Wind turbines are designed to capture a portion of the wind's kinetic energy and convert it to usable energy [14] in the form of electricity. This section presents a brief explanation of the basic operating principles of WTs.

## 1. Energy in the Wind

Wind speed is a random process that depends on several factors. The main parameter that describes the ability to extract power is the mean wind speed for the specific area of interest. The probability distribution function (PDF) of the mean wind speed  $V_m$  over an area is modeled as a Weibull distribution [14] of the form:

$$P(V_m) = \frac{k}{c} \left( \frac{V_m}{c} \right)^{k-1} e^{-\left( \frac{V_m}{c} \right)^k}, \quad (0.0)$$

where the parameters  $k$  and  $c$  are called the shape and scale factor, respectively, and are both positive real numbers.

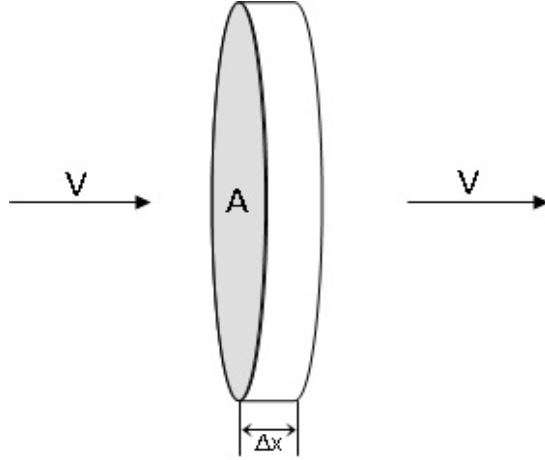


Figure 2. A volume of air flowing with speed  $V$ .

If one takes a volume of air  $A\Delta x$  flowing with speed  $V$  as shown in Figure 2, the kinetic energy stored in the wind is

$$E_k = \frac{1}{2} m V^2, \quad (0.0)$$

where  $m$  is the mass of the air.

If we replace the mass in terms of the air density  $\rho$  and the volume as  $m = \rho A \Delta x$ , Equation (2.2) can be written as

$$E_k = \frac{1}{2} \rho (A \Delta x) V^2, \quad (0.0)$$

and from Equation (2.3) one can determine the wind energy per unit volume  $A \Delta x = 1$  as

$$E_k = \frac{1}{2} \rho V^2. \quad (0.0)$$

Since the power is defined as the derivative of the energy with respect to time, one can derive an expression for the power of the wind:

$$P_v = \frac{\Delta E}{\Delta t} = \frac{\frac{1}{2} \rho (A \Delta x) V^2}{\Delta t} = \frac{1}{2} \rho A V^3. \quad (0.0)$$

## 2. Wind Turbine Aerodynamics – Disc Actuator Model

Turbine aerodynamics describes the forces developed on a wind turbine by an airflow passing through it. The approach used to derive a model for the wind turbine is actuator disc theory [14]. In this theory, the WT is regarded as an actuator disc, a device that is designed to extract part of the kinetic energy of the wind. This theory also gives a value for the maximum efficiency limit. If one assumes the disc is immersed in an airflow as shown in Figure 3, then the upstream wind speed  $V$  has to be greater than the downstream wind speed  $V_{\infty}$ .

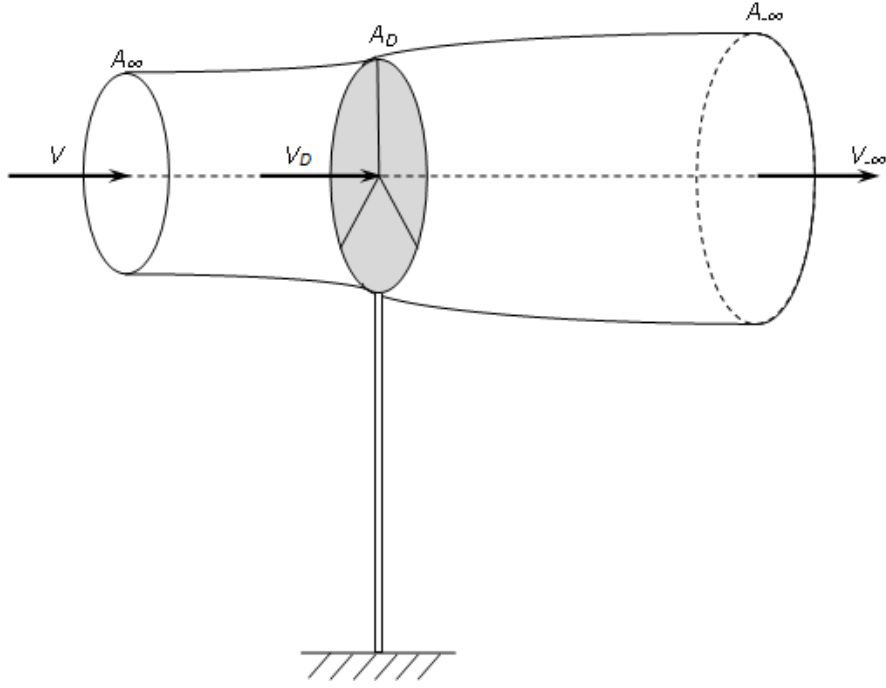


Figure 3. Actuator disc. After [14].

Furthermore, for the stream tube just enclosing the disc, the upstream cross sectional area  $A_{\infty}$  is smaller than the disc area  $A_D$ , which in turn is smaller than the downstream cross-sectional area  $A_{-\infty}$ . This happens because, by definition, due to the law of mass conservation, the mass flow must remain constant within the stream tube [14]. The above statement implies:

$$\frac{\Delta M}{\Delta t} = \text{constant} , \quad (0.0)$$

where  $\Delta M$  is the air mass going through a surface during time  $\Delta t$ . Now one can derive the following expression:

$$\frac{\Delta M}{\Delta t} = \rho A \frac{\Delta x}{\Delta t} = \rho A V = \text{constant}. \quad (0.0)$$

Therefore, if one takes ideal points away from the turbine ( $-$  and  $+$  infinity) and on the turbine, one obtains:

$$\rho A_{\infty} V = \rho A_D V_D = \rho A_{-\infty} V_{-\infty}. \quad (0.0)$$

Since the air that passes through the disc undergoes a speed reduction equal to  $V - V_{-\infty}$ , this implies a reduction in its kinetic energy. This results in a force  $F_D$  developed by the actuator disc on the incident airflow, which is given by Newton's second law of motion as the product of mass  $M$  and acceleration  $a$ :

$$F_D = \rho A_D \Delta x \frac{(V - V_{-\infty})}{\Delta t} = (V - V_{-\infty}) \rho A_D V_D. \quad (0.0)$$

The force  $F_D$  originated by the pressure drop introduced by the actuator disc can also be expressed as:

$$F_D = (p_D^+ - p_D^-) A_D, \quad (0.0)$$

where,  $p_D^+$  and  $p_D^-$  are the values of the air pressure immediately before and after the disc, as shown in Figure 4.

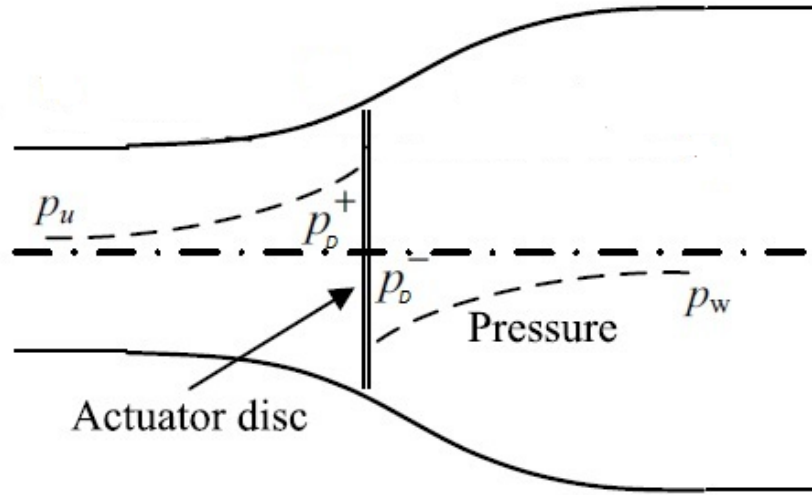


Figure 4. Pressure around actuator disk. After [15].

Since  $V_D$  is smaller than  $V$ , one can write the speed at the disc as

$$V_D = (1 - \alpha)V, \quad (0.0)$$

where one defines  $\alpha$ , with  $0 \leq \alpha \leq 1$ , which is referred to as the “axial flow interference factor.” Substituting Equation (2.11) in Equation (2.9), one gets the force  $F_D$  as:

$$F_D = (V - V_{-\infty}) \rho A_D V (1 - \alpha). \quad (0.0)$$

Equating Equations (2.10) and (2.12), one obtains:

$$(V - V_{-\infty})\rho V(1 - \alpha) = (p_D^+ - p_D^-). \quad (0.0)$$

For an airflow that is stationary, incompressible, and frictionless and with no external forces applied either upstream or downstream, the Bernoulli equation states that the total energy of the airflow remains constant. Given that the above conditions are satisfied, one can apply the Bernoulli equation from far upstream to just in front of the rotor and from just behind the rotor to far downstream [16]:

$$(p_D^+ - p_D^-) = \frac{1}{2}\rho(V^2 - V_{-\infty}^2). \quad (0.0)$$

Substituting Equation (2.14) in Equation (2.13), one finally gets

$$V_{-\infty} = (1 - 2\alpha)V, \quad (0.0)$$

and, since  $V_{-\infty}$  has to be non-negative, Equation (2.15) gives us the upper bound of  $\alpha$ , which is 0.5.

Substituting Equation (2.15) in Equation (2.12), one gets an expression for the force that is applied from the airflow on the disc:

$$F_D = 2\rho A_D V^2 \alpha(1 - \alpha). \quad (0.0)$$

The power that the actuator disc extracts from the wind is given by

$$P_D = F_D V_D = 2\rho A_D V^3 \alpha(1 - \alpha)^2. \quad (0.0)$$

This gives an idea of the maximum power available to the turbine from the flow of the wind.

A conventional way of characterizing the ability of a wind turbine to capture wind energy is the power coefficient  $C_p$  [14], which is defined as the ratio of extracted power divided by the total wind power:

$$C_p = \frac{P_D}{P_V}. \quad (0.0)$$



Substituting Equations (2.2) and (2.11) in (2.12), one gets the following expression for  $C_p$ :

$$C_p = \frac{2\rho A_d V^3 \alpha (1-\alpha)^2}{0.5\rho A_d V^3} = 4\alpha(1-\alpha)^2. \quad (0.0)$$

The power coefficient  $C_p$  is a function of the axial flow interference factor  $\alpha$ . The maximum theoretical value of the power coefficient can be found from Equation (2.19) by taking its first and second derivatives. The result, which is called the Betz limit, is  $C_{p\_max} = 0.593$  for  $\alpha$  equal to  $1/3$  [17]. This limit is valid for all kinds of wind turbines, but the actual efficiency is usually lower, and for most commercial wind turbines, a good value is between 0.40-0.50.

In practice three effects that lead to a decrease in the maximum achievable power coefficient [18]:

- Rotation of the wake behind the rotor.
- Finite number of blades and associated tip losses.
- Non zero aerodynamic drag.

### 3. Torque and Power on the Rotor

The relation between the energy of the wind flowing through the windmill and the mechanical power available at the rotor is discussed in this section. The parameter  $\beta$  is the pitch angle of the turbine blades, and  $\lambda$  the tip speed to wind speed ratio :

$$\lambda = \frac{\Omega_r R}{V}. \quad (0.0)$$

A graphical representation of the parameters involved in Equation (2.20) is shown in Figure 5.

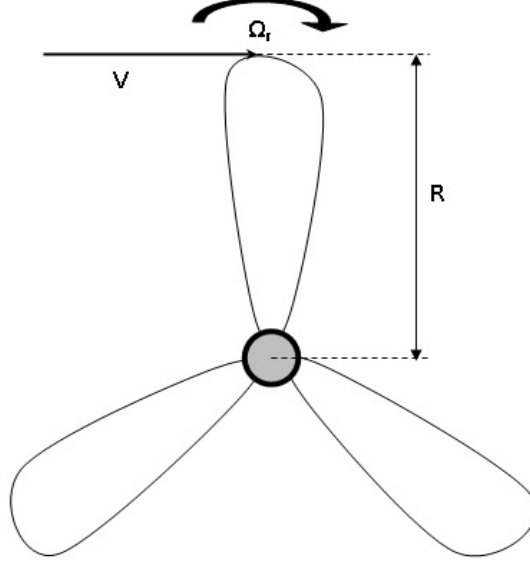


Figure 5. Turbine disc.

Substituting the expression for the power coefficient  $C_p$  from Equation (2.19) into Equation (2.17), one gets the following expression for the aerodynamic wind power:

$$P_D = 2\rho A_D V^3 \frac{C_p(\lambda, \beta)}{4} = \frac{1}{2} \rho A_D C_p(\lambda, \beta) V^3. \quad (0.0)$$

Substituting the expression for the disc area  $A_D = \pi R^2$  into Equation (2.21), one gets:

$$P_D = \frac{1}{2} \rho \pi R^2 C_p(\lambda, \beta) V^3. \quad (0.0)$$

From Equation (2.22), one can easily derive an expression for the aerodynamic torque produced by a turbine of radius  $R$  rotating at an angular rate  $\Omega_r$  with wind speed  $V$ :

$$T_r = \frac{P_r}{\Omega_r} = \frac{1}{2} \frac{\rho \pi R^2 C_p(\lambda, \beta) V^3}{\Omega_r}. \quad (0.0)$$

In Equation (2.23), the substitution of  $\Omega_r$  by its value extracted from Equation (2.20) provides the following expression:

$$T_r = \frac{1}{2} \rho \pi R^3 C_Q(\lambda, \beta) V^2 \quad (0.0)$$

where the  $C_Q$  is named the torque coefficient and is related to  $C_p$  by

$$C_q = \frac{C_p}{\lambda}. \quad (0.0)$$

In Equations (2.21) and (2.22), it can be seen that  $C_Q$  and  $C_p$  are written as functions of  $\lambda$  and  $\beta$ . However, it is assumed in this thesis that the pitch angle  $\beta=0$ , and the above coefficients are used as functions of the ratio  $\lambda$  only.

A parametric approximation of the torque coefficient  $C_Q$  is given by the following expression in terms of  $\lambda$  [7]

$$C_Q(\lambda) = \frac{a}{\lambda} \left( \frac{b}{\lambda} - 1 \right) e^{-c/\lambda}, \quad (0.0)$$

where  $a$ ,  $b$ ,  $c$  are dimensionless parameters that characterize the rotor of the wind turbine. If one substitutes Equation (2.26) in Equation (2.25), then

$$C_p(\lambda) = a \left( \frac{b}{\lambda} - 1 \right) e^{-c/\lambda}. \quad (0.0)$$

The plot of a typical power coefficient curve versus  $\lambda$  is shown in Figure 6.

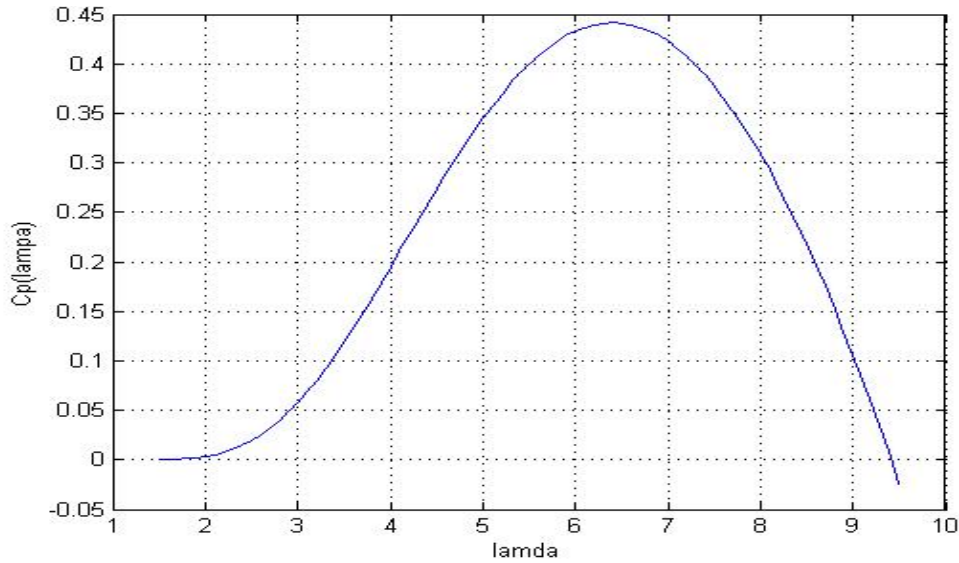


Figure 6. Typical  $C_p$  versus speed ratio  $\lambda$  curve.

The speed ratio  $\lambda$  is a very important parameter in the dynamic model of the WT. Since one wants to operate as closely as possible to maximum efficiency to have

maximum power capture and given that the wind speed cannot be controlled and the radius of the blades is fixed, one needs to vary the rotational speed of the wind turbine to keep  $\lambda$  close to its optimal value  $\lambda_{opt}$ . This is one of the advantages of variable speed WTs over fixed speed WTs, since they operate close to optimal efficiency only for a small range of wind speed values.

For a typical wind speed profile with a Weibull distribution having a shape parameter  $k = 2$  and scale parameter  $c = 8.5$ , the variable-speed turbine captures 2.3% more energy per year than the constant-speed turbine. This is considered a significant difference in the wind industry [18].

#### 4. Regions of Control

There are three different operational regions for the variable speed WTs, which are shown in Figure 7.

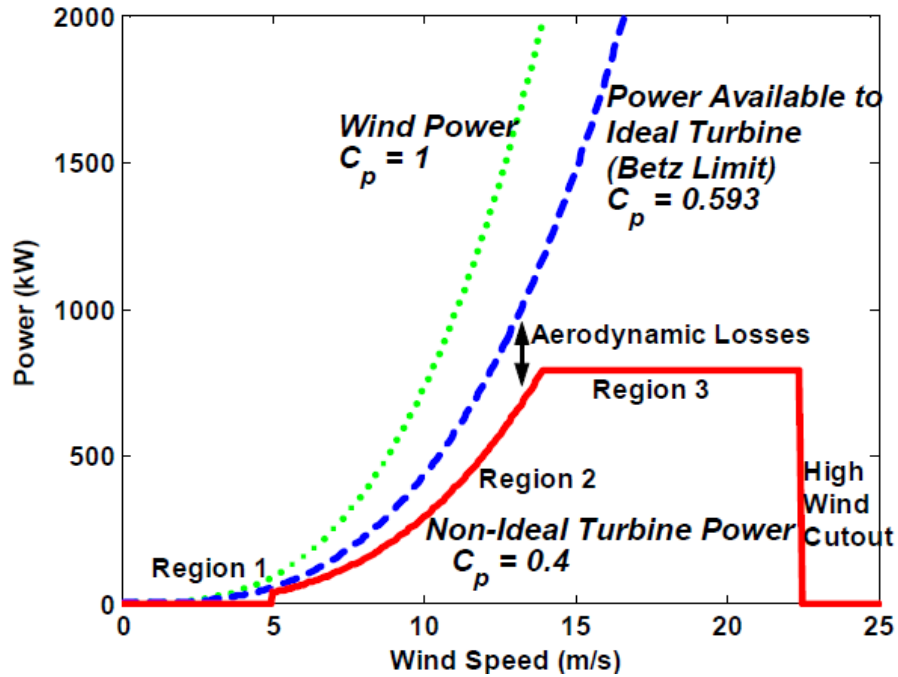


Figure 7. Example power curves for a typical commercial WT. From [5].

In region 1, the section of the solid curve, usually located to the left of 4 to 5 m/s wind speed, the power available in the wind is low compared to the losses in the turbine system; therefore, the turbine is usually not operating in this region. The use of modern control strategies is not usually critical in region 1 [5].

Region 2, illustrated by the cubic section of the red curve, is generally for winds speeds between 4 to 5 m/s up to the WT's rated wind speed, usually between 12 to 15 m/s. In this area, the WT is in operational mode, and it is desirable for it to capture as much power from the wind as possible. The goal in this region is to approach the Betz Limit curve as closely as possible.

Region 3 is for operation above rated wind speed of the WT, i.e., the wind speed above which maximum peak power is produced. The goal of control strategies applied in this region is to limit the wind power captured so as not to exceed the designed electrical and mechanical load limits of the system.

All research in this thesis centers on Region 2.

## **B. DOUBLY-FED INDUCTION GENERATOR (DFIG)**

Induction machines are used in a wide variety of applications and are, without doubt, the workhorse of the electric power industry [19].

An induction motor is an electric motor that is driven by alternating current (AC). It consists of two basic parts: the stator, which is on the outside and has windings supplied with AC to produce a rotating magnetic field, and the rotor, which is attached to the output shaft on the inside. When balanced multi-phase currents flow through the stator windings, a rotating air-gap magnetomotive force (MMF) is produced, and, if the rotor rotates at different speed than the speed of the rotating MMF, balanced multi-phase currents are induced in the rotor windings. There are two different types of rotor windings: wound and squirrel cage. In Figure 8 the cross section of a typical three-phase induction machine with a squirrel cage rotor is illustrated.

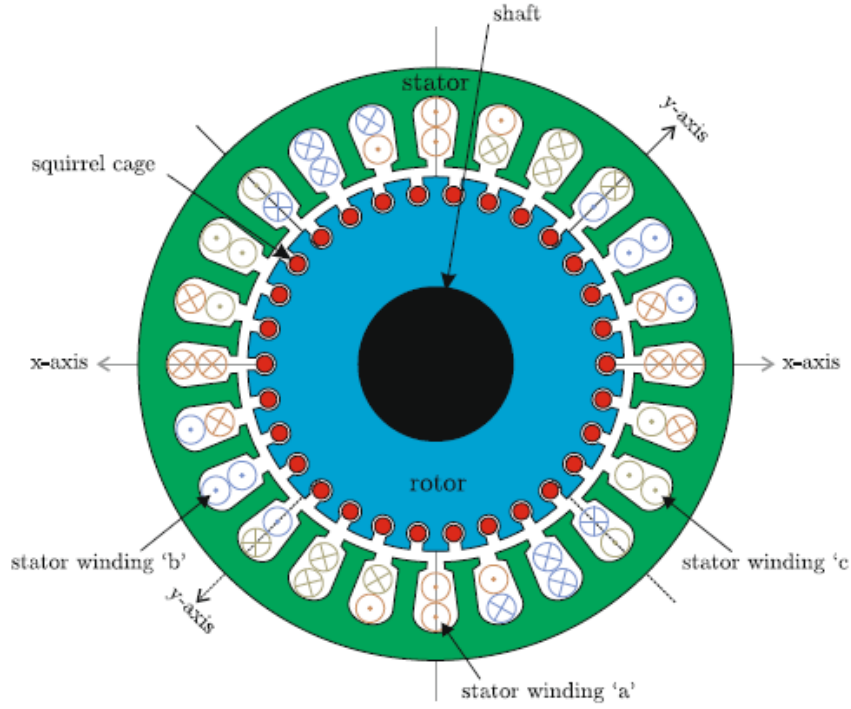


Figure 8. Induction machine cross section. From [20].

In single-fed induction generators, the rotor windings are short-circuited, while DFIGs take full advantage of both stator and rotor excitations. The rotor currents and voltages of the DFIG are at the basis of the control techniques developed in this thesis.

## 1. Reference Frames – Dynamic Models

Three phase signals (currents or voltages) can be represented either by the respective time domain components (called “abc”) or, more conveniently, by the expansion with respect to a rotating reference frame (called “qd0”).

The equations converting time domain “abc” voltages into “qd0” components and vice versa are very standard and can be found in a number of sources [12], [19].

In the “qd0” reference frame for a symmetrical DFIG, we have the following equations for the flux linkages from [19]:

$$\begin{aligned}
p\lambda_{qd0s} &= -r_s i_{qd0s} - j\omega \lambda_{dq0s} + v_{qd0s} \\
p\lambda'_{qd0r} &= -r'_r i'_{qd0r} + j(\omega - \omega_r) \lambda'_{qd0r} + v'_{qd0r},
\end{aligned} \tag{0.0}$$

where  $v$ ,  $i$ ,  $\lambda$  refer to voltages, current, and flux linkages in the qd0 reference frame of the stator (subscript  $s$ ) and the rotor (subscript  $r$ ). The parameter  $\omega$  is the electrical angular rate of the reference frame, determined by the line frequency (say 60 Hz in the USA);  $\omega_r$  is the electrical frequency of the rotor circuit;  $r_s, r_r$  are the stator and rotor resistances; and  $p$  stands for the differential operator  $d/dt$ .

Any qd0 variable, say  $f$ , can be expressed in a complex form as:

$$f_{qd0} = f_q - jf_d + 0. \tag{0.0}$$

Therefore, the flux linkages are defined as:

$$\begin{aligned}
(\lambda_{dq0s})^T &= [\lambda_{ds} \quad -\lambda_{qs} \quad 0] \\
(\lambda'_{dq0r})^T &= [\lambda'_{dr} \quad -\lambda'_{qr} \quad 0]^T,
\end{aligned} \tag{0.0}$$

where the flux components are related to the currents by standard equations [19]

$$\begin{aligned}
\lambda_{qs} &= L_s i_{qs} + L_M (i_{qs} + i'_{qr}) \\
\lambda_{ds} &= L_s i_{ds} + L_M (i_{ds} + i'_{dr}) \\
\lambda_{0s} &= L_s i_{0s} \\
\lambda_{qr} &= L'_r i'_{qr} + L_M (i_{qs} + i'_{qr}) \\
\lambda_{dr} &= L'_r i'_{dr} + L_M (i_{ds} + i'_{dr}) \\
\lambda_{0r} &= L'_r i'_{0r}
\end{aligned} \tag{0.0}$$

Expanding Equations (2.28) and combining them with Equations (2.31), one gets the following set of equations to characterize the DFIG [19]:

$$\begin{bmatrix} v_{qs} \\ v_{ds} \\ v_{0s} \\ v_{qr} \\ v_{dr} \\ v_{0r} \end{bmatrix} = \begin{bmatrix} r_s + \frac{p}{\omega_b} X_{ss} & \frac{\omega}{\omega_b} X_{ss} & 0 & \frac{p}{\omega_b} X_M & \frac{\omega}{\omega_b} X_M & 0 \\ -\frac{\omega}{\omega_b} X_{ss} & r_s + \frac{p}{\omega_b} X_{ss} & 0 & -\frac{\omega}{\omega_b} X_M & \frac{p}{\omega_b} X_M & 0 \\ 0 & 0 & r_s + \frac{p}{\omega_b} X_{ls} & 0 & 0 & 0 \\ \frac{p}{\omega_b} X_M & \left( \frac{\omega - \omega_r}{\omega_b} \right) X_M & 0 & r_r' + \frac{p}{\omega_b} X_{rr}' & \left( \frac{\omega - \omega_r}{\omega_b} \right) X_{rr}' & 0 \\ -\left( \frac{\omega - \omega_r}{\omega_b} \right) X_M & \frac{p}{\omega_b} X_M & 0 & -\left( \frac{\omega - \omega_r}{\omega_b} \right) X_{rr}' & r_r' + \frac{p}{\omega_b} X_{rr}' & 0 \\ 0 & 0 & 0 & 0 & 0 & r_r' + \frac{p}{\omega_b} X_{lr}' \end{bmatrix} \begin{bmatrix} i_{qs} \\ i_{ds} \\ i_{0s} \\ i_{qr} \\ i_{dr} \\ i_{0r} \end{bmatrix} \quad (0.0)$$

where

$$\begin{aligned} X_{ss} &= X_{ls} + X_M \\ X_{rr}' &= X_{lr}' + X_M \\ X_{ls} &= \omega_b L_{ls} \\ X_{lr}' &= \omega_b L_{lr}' \\ X_M &= \omega_b L_M \end{aligned} \quad (0.0)$$

express all the impedances. In the above equations,  $\omega_b$  is the base or rated frequency (say the standard 60 Hz);  $\omega_r$  is the electrical rotational frequency of the rotor; and  $\omega_e$  is the electrical rotational frequency of the stator. The variables  $L_{ls}$  and  $L_M$  are the leakage and magnetizing inductances of the stator windings, and  $L_{lr}'$  is the leakage inductance for the rotor windings. Also, as mentioned,  $r_s$  and  $r_r'$  are the stator and the rotor resistances.

The electromagnetic torque of the generator is given by the following expressions [19], which are all equivalent:

$$T_e = \left( \frac{3}{2} \right) \left( \frac{P}{2} \right) L_M (i_{qs} i_{dr}' - i_{ds} i_{qr}'), \quad (0.0)$$

$$T_e = \left( \frac{3}{2} \right) \left( \frac{P}{2} \right) L_M (\lambda_{qr}' i_{dr}' - \lambda_{dr}' i_{qr}') \quad (0.0)$$

$$T_e = \left( \frac{3}{2} \right) \left( \frac{P}{2} \right) L_M (\lambda_{ds} i_{qs} - \lambda_{qs} i_{ds})$$

In the above expressions,  $P$  is the number of magnetic poles of the generator, and  $T_e$  is positive for motor action and negative for generator action.



The total real and reactive power of a three-phase balanced DFIG in steady state conditions is given by [19]:

$$\begin{aligned} P_e &= \frac{3}{2}(V_{qs}I_{qs} + V_{ds}I_{ds}) \\ Q_e &= \frac{3}{2}(V_{qs}I_{ds} - V_{ds}I_{qs}) \end{aligned} \quad (0.0)$$

## 2. DFIG Model

Equations (2.28) clearly define a nonlinear dynamic system where the fluxes  $\lambda$  are the states and the voltages are the control signals. Equivalently, from [19], one can redefine the states in terms of the  $qd0$  current components of the stator and the rotor.

The whole system is a nonlinear dynamic system and was implemented by Professor A. Julian in Simulink [21], as shown in Figure 9. The time domain voltage components  $v_a, v_b, v_c$  of the stator and the rotor are explicitly shown, together with the state variables  $i_a, i_b, i_c$  of stator and rotor, in the time domain. In addition, other physical quantities, like the torque on the load  $T_L$ , are shown, along with all relevant power components  $P_e$  (active) and  $Q_e$  (reactive). The model of the DFIG is described in more detail in [21].

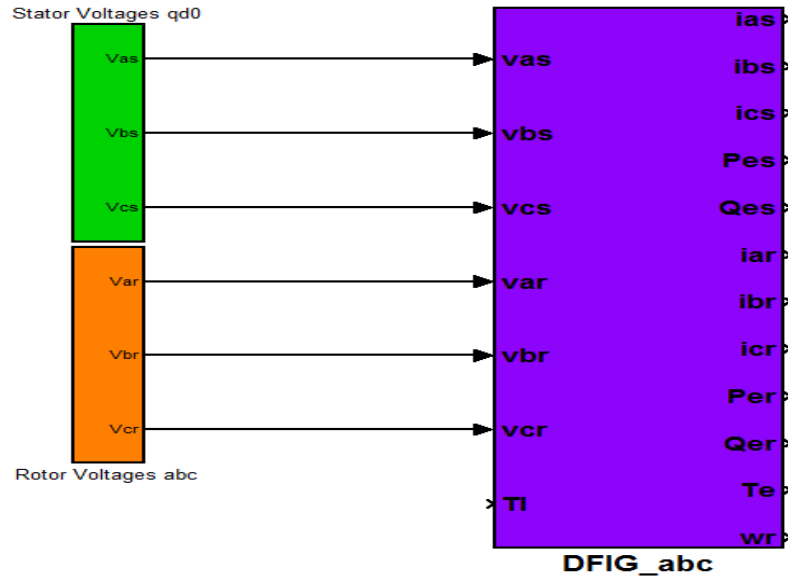


Figure 9. General view of the DFIG model.

This model is used extensively in the next chapters, both as a benchmark for simulating the dynamics of the DFIG and as the basis of the analytical design of the proposed algorithms.

## **C. CHAPTER SUMMARY**

The basic theory behind WTs and DFIGs was presented in this chapter, and a description of the simulation model for a DFIG was provided. The quality of the model is of great importance, because the effectiveness of the controller depends on it. In the next chapter, three different algorithms of online parameter identification will be presented.

THIS PAGE INTENTIONALLY LEFT BLANK

### III. ONLINE PARAMETER ESTIMATION

#### A. INTRODUCTION

The mathematical model described in the Chapter II, with its Simulink implementation, is representative of the DFIG physical system. In general, the various parameters defined (resistances and inductances) have to be estimated based on voltage and the current measurements of the physical system itself. The mathematical model can be used for control design and validation by computer simulation.

The purpose of this chapter is to describe the methods used to achieve on-line estimation of the DFIG parameters. The essential idea behind on-line estimation is the comparison of the observed system response  $y(t)$  with the output of a parameterized model whose structure is the same as that of the plant model [22]. In this case, the output vector  $y(t)$  consists of all the measured currents in the qd0 reference frame under different conditions of excitation through the input voltages.

The parameter vector  $\theta(t)$  contains estimates of all the parameters in the state space model in Chapter II, and it is adjusted continuously so that  $\hat{y}(\theta, t)$  approaches  $y(t)$  as  $t$  increases. Under certain input conditions,  $\hat{y}(\theta, t)$  being close to  $y(t)$  implies that  $\hat{\theta}(t)$  is close to the unknown parameter vector  $\theta(t)$  of the plant model. The online estimation procedure, therefore, involves three steps [22]:

- Create an appropriate parameterization of the plant model;
- Design an algorithm for generating and updating the parameter vector estimate; and
- Properly excite the plant such that the parameter estimates approach the actual expected values as  $t \rightarrow \infty$ .

In general, the plant model of a system to be studied for identification should be expressed in the following form:

$$\underline{y}(t) = \underline{\Phi}^T(t) \underline{\theta}(t), \quad (0.0)$$

which can be explicitly written as:

$$\begin{bmatrix} y_1(t) \\ y_2(t) \\ \vdots \\ y_n(t) \end{bmatrix} = \begin{bmatrix} \varphi_{11}(t) & \varphi_{12}(t) & \cdot & \cdot & \cdot & \varphi_{1m}(t) \\ \varphi_{21}(t) & \cdot & \cdot & \cdot & \cdot & \cdot \\ \cdot & \cdot & \cdot & \cdot & \cdot & \cdot \\ \cdot & \cdot & \cdot & \cdot & \cdot & \cdot \\ \varphi_{n1}(t) & \cdot & \cdot & \cdot & \cdot & \varphi_{nm}(t) \end{bmatrix} \begin{bmatrix} \theta_1(t) \\ \theta_2(t) \\ \cdot \\ \cdot \\ \cdot \\ \theta_m(t) \end{bmatrix}, \quad (0.0)$$

where the  $n \times 1$  vector  $\underline{y}(t)$  consists of the observed variables; the  $m \times 1$  vector  $\underline{\theta}(t)$  consists of the unknown parameters to be determined; and the  $n \times m$  matrix  $\underline{\Phi}^T(t)$  consists of known functions that describe the plant model, which are called regression variables[23]. In this thesis, as one can see later on,  $n=6$  and  $m=5$ .

It is shown in [22], [23] that under conditions of persistency of excitation, the estimated parameters converge to the true parameters. Loosely speaking, this is satisfied when the signal is sufficiently excited so that the input-output behavior can be modeled by a unique parameter vector.

## B. SYSTEM EQUATIONS

Based on what was discussed in the previous section, one needs to rewrite the dynamic equations in terms of parameters and regression vectors. In particular, the five quantities that form the parameter vector  $\theta$  to be estimated are the following:

$$\theta = \begin{bmatrix} r_s & r_r' & L_{ls} & L_{lr}' & L_M \end{bmatrix}^T. \quad (0.0)$$

The vector  $y(t)$  of observations is defined by the stator and rotor voltages:

$$y(t) = v(t) = \begin{bmatrix} v_{qs} & v_{ds} & v_{0s} & v_{qr} & v_{dr} & v_{0r} \end{bmatrix}^T. \quad (0.0)$$

Substituting Equations (3.3) and (3.4) in Equation (2.32), one obtains:

$$v(t) = \begin{bmatrix} i_{qs} & 0 & pi_{qs} + \omega i_{ds} & 0 & p(i_{qs} + i'_{qr}) + \omega(i_{ds} + i'_{dr}) \\ i_{ds} & 0 & pi_{ds} - \omega i_{qs} & 0 & p(i_{ds} + i'_{dr}) - \omega(i_{qs} + i'_{qr}) \\ i_{0s} & 0 & pi_{0s} & 0 & 0 \\ 0 & i'_{qr} & 0 & pi'_{qr} + (\omega - \omega_r)i'_{dr} & p(i_{qs} + i'_{qr}) + (\omega - \omega_r)(i_{ds} + i'_{dr}) \\ 0 & i'_{dr} & 0 & pi'_{dr} - (\omega - \omega_r)i'_{qr} & p(i_{ds} + i'_{dr}) - (\omega - \omega_r)(i_{qs} + i'_{qr}) \\ 0 & i'_{0r} & 0 & pi'_{0r} & 0 \end{bmatrix} \theta(t), \quad (0.0)$$

where the matrix on the right of Equation (3.5) becomes  $\Phi^T(t)$  in Equation(3.2):

$$v(t) = \Phi^T(t)\theta(t), \quad (0.0)$$

and  $\omega$  is the angular velocity of the arbitrary reference frame that was chosen.

## C. ESTIMATORS

In order to estimate the machine parameters vector  $\theta(t)$ , three different identification approaches were used:

- least mean squares (LMS),
- recursive least Squares (RLS), and
- recursive least squares with exponential forgetting (RLS-EF).

The next section describes the three different estimators.

### 1. Least Mean Squares (LMS)

The first estimation algorithm is based on the Least Mean Squares (LMS) method. This was initially formulated at the end of the 18th century by the German mathematician and scientist K. F. Gauss to calculate the orbits of planets and asteroids. From [23], using the above method, the parameters of the model should be chosen in such a way that the sum of squares of the differences between the observed and computed values, multiplied by numbers that measure the degree of precision, is a minimum.

*a. Equations Setup*

Based on the model described in Equation (3.1), one can define the prediction or estimation error  $e(t)$  [23], as the difference between  $\hat{y}(t)$  and  $y(t)$  :

$$\underline{e}(t) = \underline{y}(t) - \underline{\hat{y}}(t) = \underline{y}(t) - \Phi^T(t)\underline{\hat{\theta}}(t) . \quad (0.0)$$

In addition, one can define the parameter error  $\tilde{\theta}(t)$  as follows:

$$\tilde{\theta}(t) = \theta(t) - \hat{\theta}(t) . \quad (0.0)$$

Thus, from Equations (3.1), (3.7) and (3.8), one can derive the following expression for  $e(t)$ :

$$e(t) = \Phi^T(t)\tilde{\theta}(t) . \quad (0.0)$$

From [24], the general form of an identification algorithm is defined by a differential equation, called the update law, which is of the form:

$$\dot{\tilde{\theta}}(t) = F\{y(t), e(t), \tilde{\theta}(t), \Phi(t)\} . \quad (0.0)$$

By the standard steepest descent algorithm, one can obtain the following expression for the derivative of  $\tilde{\theta}(t)$  with respect to time:

$$\dot{\tilde{\theta}}(t) = -\mu\Phi(t)e(t) , \quad (0.0)$$

where  $\mu$  is an arbitrarily chosen strictly positive parameter called the adaptation gain and allows for a variable rate of adaptation of the parameters. The greater the value of  $\mu$ , the faster the convergence, but the response is more sensitive to noise and might induce oscillations in the system.

To analyze the behavior of this system, one can define a Lyapunov function:

$$V(\theta(t)) = \frac{1}{2} \|\tilde{\theta}(t)\|^2 . \quad (0.0)$$

According to [25], for  $\tilde{\theta}(t)$  to converge, the Lyapunov function described in Equation (3.12) has to be positive definite, and its total derivative with respect to time must be negative semi-definite. By definition, it is positive definite, since in this case the parameters are positive real numbers and this case takes the norm of the parameter vector. The derivative with respect to time of  $V(\theta(t))$  is given by:

$$\dot{V}(\theta(t)) = \frac{dV(\theta(t))}{dt} = \tilde{\theta}^T(t) \dot{\tilde{\theta}}(t). \quad (0.0)$$

Substituting the expression of  $\dot{\tilde{\theta}}(t)$  from Equation (3.11) into Equation (3.13), one can obtain:

$$\dot{V}(\theta, t) = -\mu \tilde{\theta}^T(t) \Phi(t) e(t). \quad (0.0)$$

Since the prediction error  $e(t)$  is related to the parameter error by Equation (3.9), one can obtain:

$$\dot{V}(\theta, t) = -\mu \tilde{\theta}^T(t) \Phi(t) \Phi^T(t) \tilde{\theta}(t) = -\mu \|\Phi^T(t) \tilde{\theta}(t)\|^2 \leq 0. \quad (0.0)$$

The outcome of Equation (3.15) is that  $\dot{V}(\theta, t)$  is negative semi-definite, and as a result,  $\|\tilde{\theta}(t)\|$  decreases monotonically with time. Under conditions of persistency of excitation, this implies that the parameter error actually converges to zero as:

$$\theta(t) - \hat{\theta}(t) \rightarrow 0. \quad (0.0)$$

Since the system parameter vector  $\theta(t)$  is assumed constant or slowly changing with time, one can assume that  $\dot{\theta}(t) \approx 0$ . Therefore, by differentiating Equation (3.8) and substituting Equation (3.11), one gets the following expression for the derivative of the parameter estimates:

$$\dot{\hat{\theta}}(t) = -\dot{\tilde{\theta}}(t) = \mu \Phi(t) e(t). \quad (0.0)$$

Integrating Equation (3.17), one gets the expression needed for the estimates:



$$\hat{\theta}(t) = \hat{\theta}(0) + \int_0^t \mu \Phi(\tau) [y(\tau) - \Phi^T(\tau) \hat{\theta}(\tau)] d\tau, \quad (0.0)$$

where the initial condition can be arbitrarily chosen based on any a priori knowledge of the plant.

### b. Implementation

The simulation of this estimation method required the creation of a Simulink subsystem which was added to the model described in Chapter II for the DFIG. A general view of the estimator is shown in Figure 10.

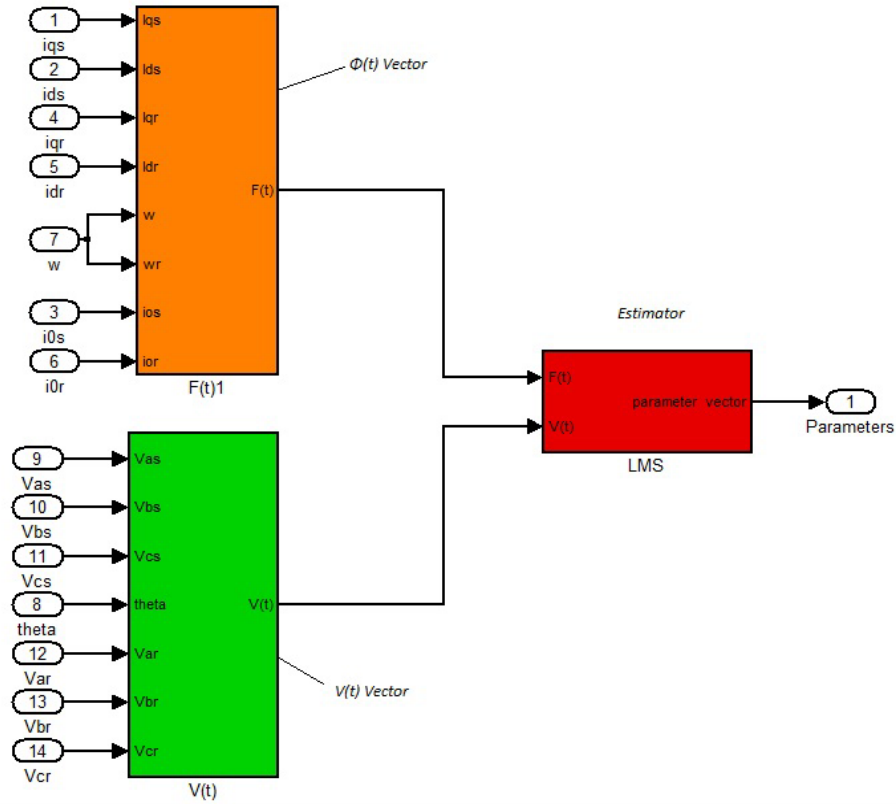


Figure 10. General view of the LMS estimation model.

The Simulink blocks that provide the vectors  $\Phi(t)$  and  $V(t)$  are common for all the different methods and were implemented using Equations (3.6). These are the equations for reference frame transformation described in [19]. The estimator block for the LMS is shown in more detail in Figure 11.

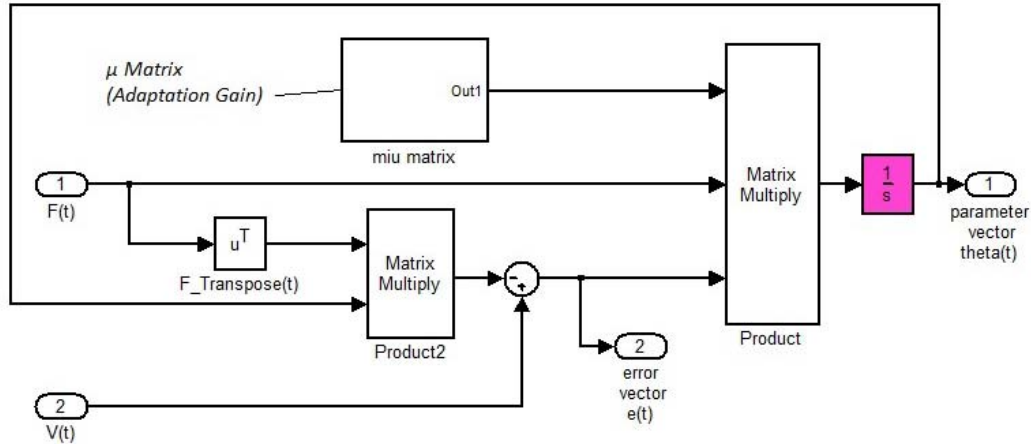


Figure 11. Detailed block diagram for the LMS estimator model.

It can be seen in Figure 11 that instead of using the same adaptation gain  $\mu$  for all the parameters, different values of  $\mu$  for the different channels were employed. The adaptation matrix in Figure 11 is a diagonal matrix of the form:

$$\mu\_Matrix = \begin{bmatrix} \mu_{11} & 0 & 0 & 0 & 0 \\ 0 & \mu_{22} & 0 & 0 & 0 \\ 0 & 0 & \mu_{33} & 0 & 0 \\ 0 & 0 & 0 & \mu_{44} & 0 \\ 0 & 0 & 0 & 0 & \mu_{55} \end{bmatrix} .$$

The reason behind this is to compensate for different scaling factors and bring all the signals to a similar order of magnitude. This seems to improve the convergence rate and prevent instability.

The values of the non-zero terms in the  $\mu$  matrix were chosen to create a relatively fast convergence without affecting the stability of the system. Large values of the parameters  $\mu_{ii}$  lead to fast convergence, but the estimates are oscillating. Very small values lead to very slow but stable convergence. To illustrate, the values chosen for the above parameters that gave a stable output are shown in Table 1.

Table 1. Adaptation gains for the LMS simulation.

$\mu_{ii}$	Value
$\mu_{11}$	130
$\mu_{22}$	820
$\mu_{33}$	0.007
$\mu_{44}$	0.38
$\mu_{55}$	0.0135

## 2. Recursive Least Squares (RLS)

The second method was recursive least squares (RLS).

### a. Equations Setup

This method is implemented in discrete time and recursively computes the parameter estimates  $\hat{\theta}(n)$  by minimizing the quadratic error [23]:

$$V(\theta, n) = \frac{1}{2} \sum_{i=1}^n [y(iT_s) - \Phi^T(iT_s)\hat{\theta}]^2, \quad (0.0)$$

with  $T_s$  as the sampling interval.

From [26], the recursive estimate can be interpreted as a Kalman Filter for the process:

$$\begin{aligned} \hat{\theta}(n+1) &= \hat{\theta}(n) \\ y(n) &= \Phi^T(n)\hat{\theta}(n) + e(n) \end{aligned}, \quad (0.0)$$

where  $y(n)$   $\Phi(n)$  are given by Equation (3.4) and Equation (3.6), respectively, by substituting  $t$  with  $n$ .

The recursive equations for the RLS can then be derived from the Kalman filter equations used in [27]:

$$\begin{aligned}
\hat{\theta}(n+1) &= \hat{\theta}(n) + K(n)[y(n+1) - \Phi^T(n+1)\hat{\theta}(n)] \\
K(n) &= P(n)\Phi(n+1)[\Phi^T(n+1)P(n)\Phi(n+1) + I]^{-1} \quad , \\
P(n+1) &= P(n) - K(n)[\Phi^T(n+1)P(n)\Phi(n+1) + I]^{-1}K^T(n)
\end{aligned} \tag{0.0}$$

where the matrix  $\Phi(n)$  has to be full rank, which means that it has to be nonsingular for all  $n > 0$ . The initial condition for Equations (3.21) is:

$$P(0) = \sigma^2 I_{m \times m}, \tag{0.0}$$

where  $\sigma$  is a positive number, much higher than the parameters, and  $m$  is the dimension of  $y(t)$ , which in this case is six.

### b. Implementation

The general outlook of the RLS estimator is shown in Figure 12.

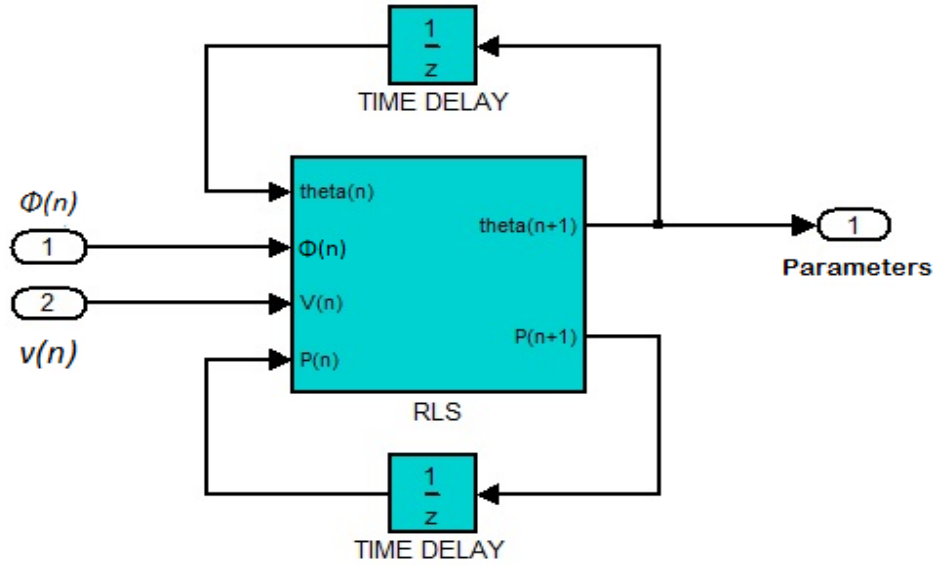


Figure 12. General view of RLS estimator model.

A more detailed view of the inside of the RLS block is shown in Figure 13. The inputs to the block are  $\Phi(n)$  and  $v(n)$ , and the output is the parameter vector estimates  $\hat{\theta}(n+1)$ .

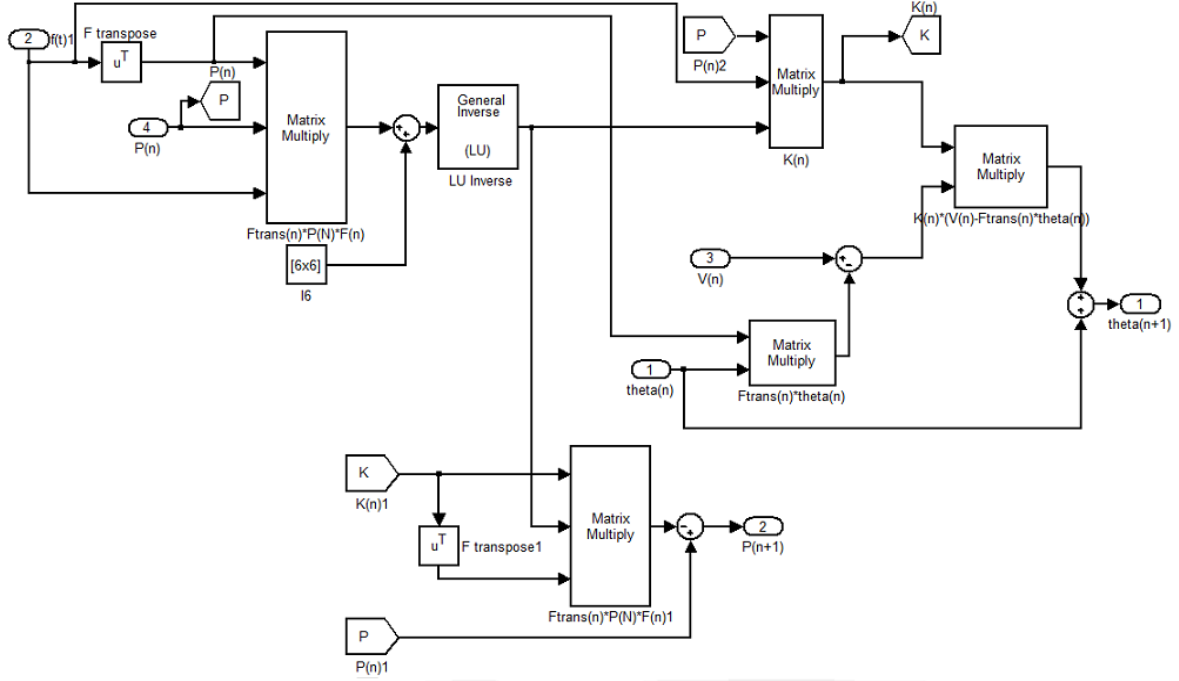


Figure 13. Detailed view of RLS estimator model.

### 3. RLS With Exponential Forgetting (RLS-EF)

In the above estimations, the parameters are assumed constant or slowly changing. Now consider the case of varying parameters from either environmental or operational conditions or a change in the parameters due to a fault in the system. The case that is of more interest is when the parameters are slowly changing in time. In this case, one needs to design an algorithm with a “forgetting factor” which discounts data exponentially further back in time.

#### a. Equations Setup

According to [23], the RLS-EF algorithm is obtained by changing the cost function of Equation (3.19) from the one that was used for the RLS algorithm to the following:

$$V(\theta, t) = \frac{1}{2} \sum_{i=1}^t \lambda^{t-i} [y(i) - \Phi^T(i) \hat{\theta}(i)]^2, \quad (0.0)$$

where  $\lambda$  is a parameter such that  $0 < \lambda \leq 1$  and is called the forgetting factor. The meaning of Equation (3.23) is that one weights the last data by 1, with a factor of  $\lambda^n$  for data that are  $n$  time units old. This means that one reduces exponentially the weight of each set of measurements. Thus, the equation for the RLS with exponential forgetting becomes:

$$\begin{aligned}\hat{\theta}(t+1) &= \hat{\theta}(t) + K(t)[y(t+1) - \Phi^T(t+1)\hat{\theta}(t)] \\ K(t) &= \frac{P(t)}{\lambda} \Phi(t+1) [\Phi^T(t+1) \frac{P(t)}{\lambda} \Phi(t+1) + I]^{-1} \\ P(t+1) &= \frac{P(t)}{\lambda} - K(t) [\Phi^T(t+1) \frac{P(t)}{\lambda} \Phi(t+1) + I]^{-1} K^T(t)\end{aligned}\quad (0.0)$$

#### ***b. Implementation***

The general outlook of the RLS-EF estimator is similar to that shown in Figure 12.

### **D. SIMULATION OF THE ESTIMATORS**

#### **1. Equipment**

The three estimators described in the previous pages were simulated using Simulink software. A Matlab code was created to initialize the models. The code used for initialization of the simulation models in Simulink is presented in the Appendix. To determine how well the estimators perform, one has to choose a DFIG with known parameters for comparison. The DFIG that was used is the Lab-Volt model 8231, which is a 175 W, 120 V, 60 Hz, 4-pole machine. The system parameters were used to effectively model the system in Simulink. Both the stator and rotor of that machine consist of 3-phase wye-connected windings and a stator to rotor turns ratio  $N_s/N_r = 10$ .

To have an input to determine the values of the estimated parameters required use of the values that were measured in [28] after a DC test, a no load test, and a blocked rotor test on the generator mentioned above. The results are given in Table 2.

Table 2. Measured DFIG parameters. From [28].

Parameters $\theta(t)$	Values
$r_s$	12[ $\Omega$ ]
$r_r'$	15[ $\Omega$ ]
$L_{ls}$	0.0241[H]
$L_{lr}'$	0.0241[H]
$L_M$	0.3342[H]

## 2. Simulation Results

After conducting a large number of simulations, varying the conditions and some parameters of the system, it turned out that only the first two methods gave satisfactory results. The simulation using RLS-EF method was leading the estimator to an unstable output after a period. The next section describes the results of the first two methods.

### *a. Simulation Using LMS*

The results for the parameter convergence using LMS are shown in Figures 14, 15 and 16, where the initial condition for the estimator was set to zero. The sampling time for all the simulations was set equal to 0.1 *ms*.

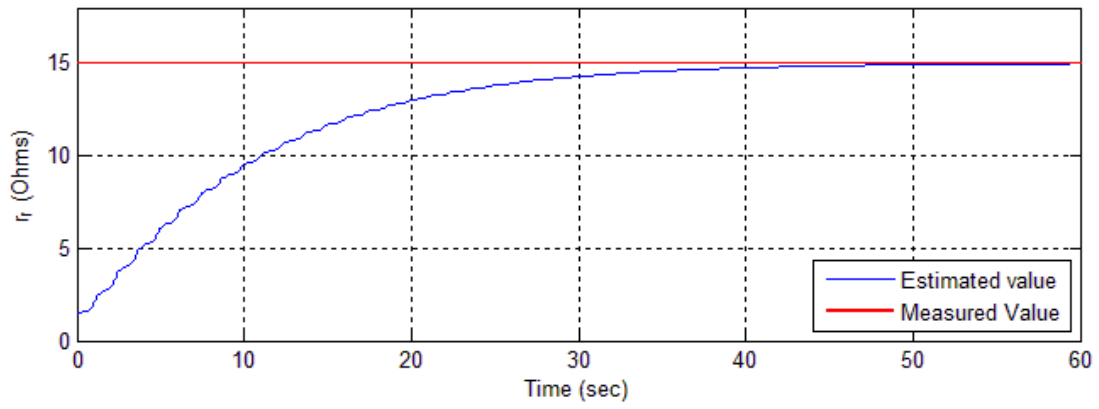
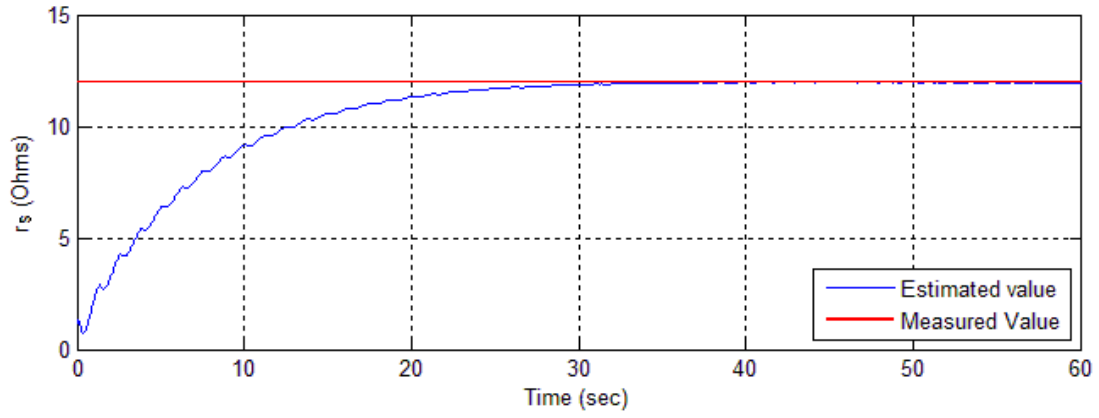


Figure 14. Convergence of  $r_s$  and  $r_r'$  using LMS from simulation.

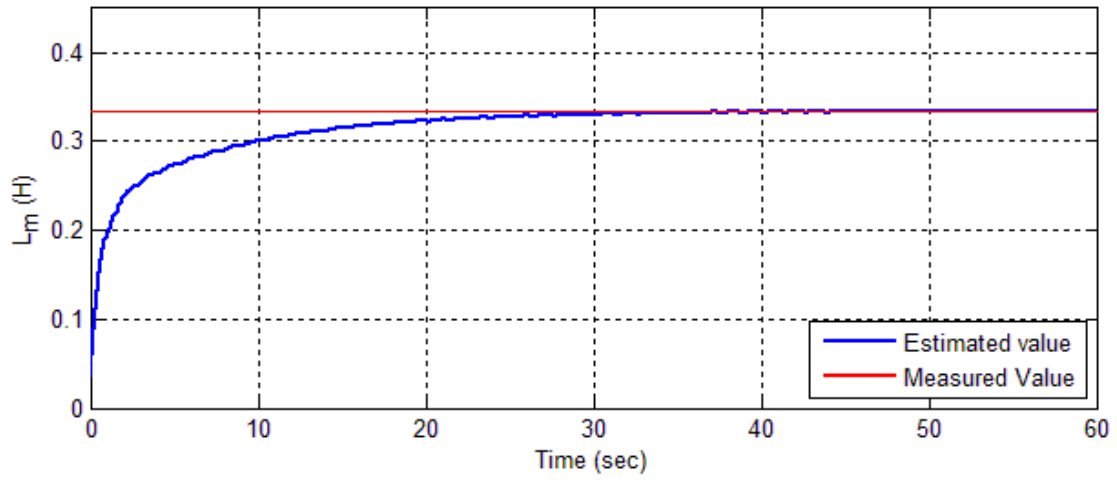


Figure 15. Convergence of  $L_m$  using LMS from simulation.



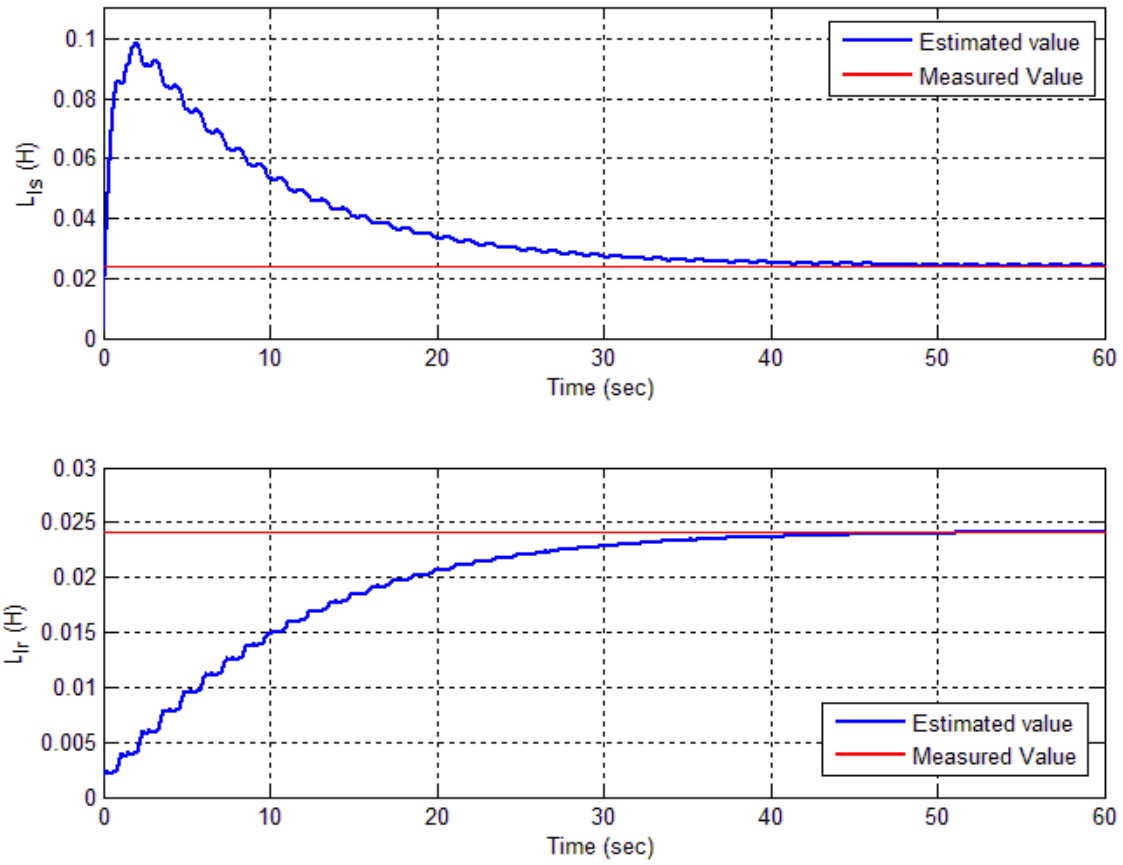


Figure 16. Convergence of  $L_{ls}$  and  $L_{lr}'$  using LMS from simulation.

One can see that the parameter estimates converge to the expected values, but it takes a while for them to settle down. This is a result that depends on the non zero values of the adaptation matrix given in Table 1. If one sets the values of initial condition vector closer to the measured values, then the convergence is much faster.

#### ***b. Simulation Using RLS***

The results of the simulation using RLS are shown in Figures 17, 18 and 19.

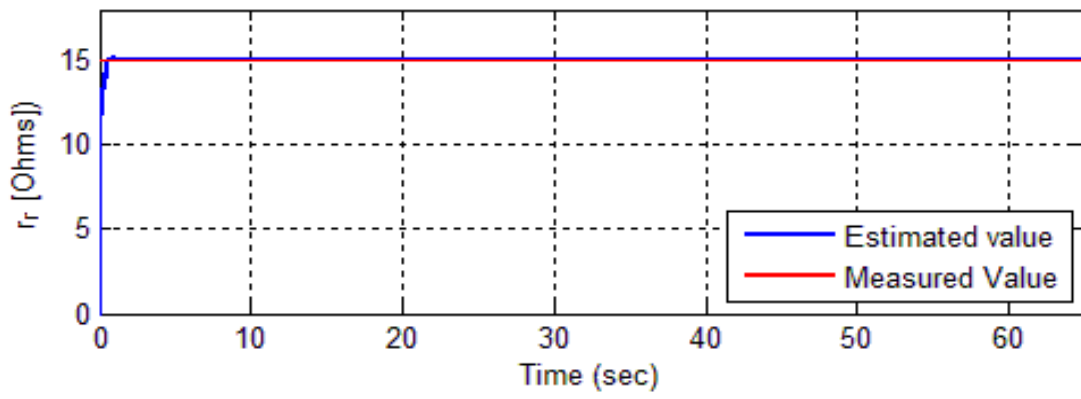
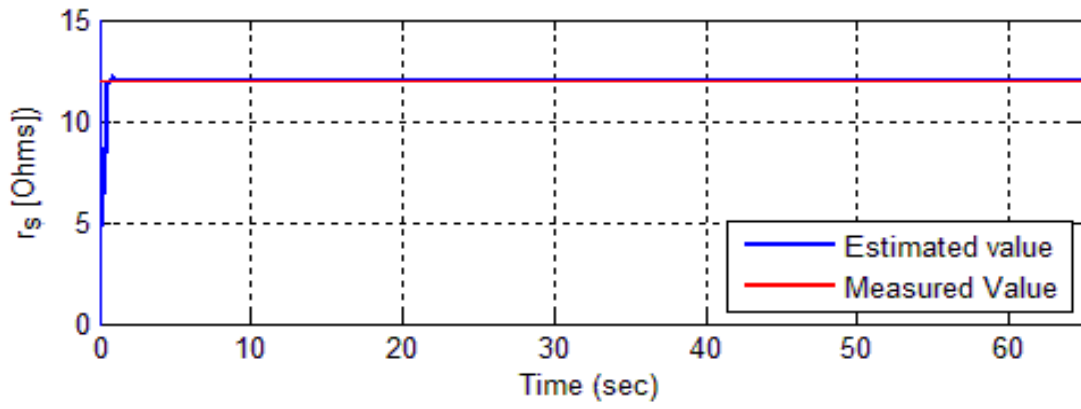


Figure 17. Convergence of  $r_s$  and  $r_r'$  using RLS from simulation.

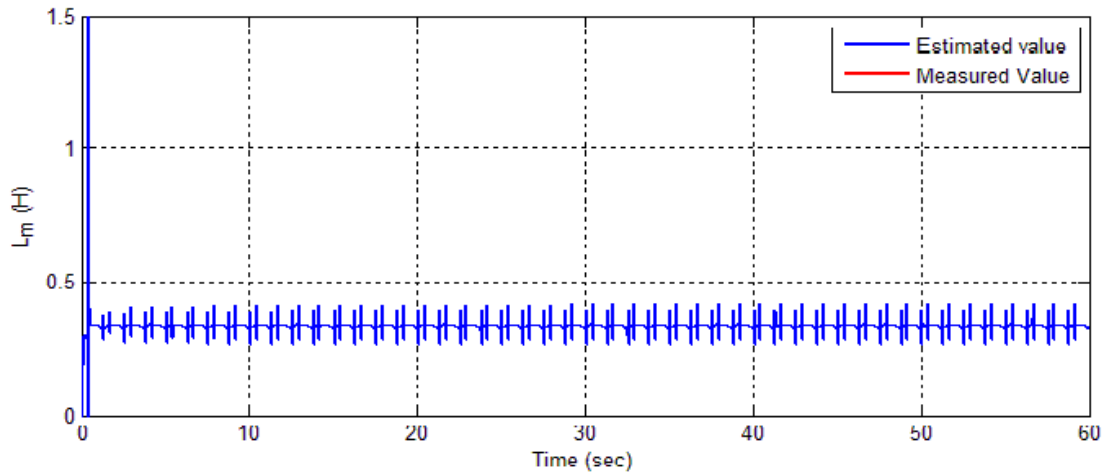


Figure 18. Convergence of  $L_m$  using RLS from simulation.

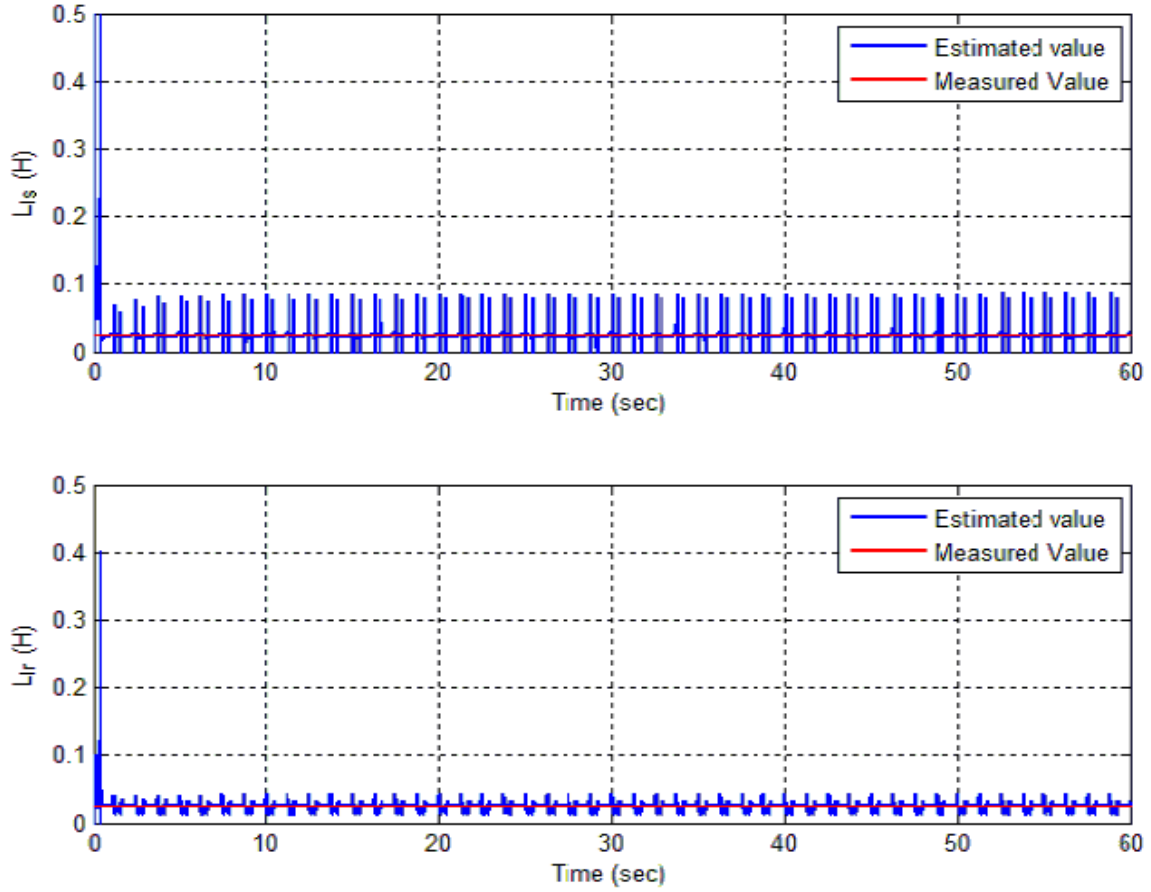


Figure 19. Convergence of  $L_{ls}$  and  $L_{lr}'$  using RLS from simulation.

From Figures 17 to 19, one can conclude that the parameter convergence using RLS is almost instantaneous, but for the inductances, the estimates oscillate around the expected values. On the other hand, the estimates for the resistances are extremely close to the experimentally measured parameter values.

## E. CHAPTER SUMMARY

In this chapter, different algorithms for system identification were presented analytically and simulated. Based on the results and given the fact that the nature of the system is relatively slow, one can say that the LMS is more suitable in this application since it performs well and provides relatively fast convergence. In the next chapter, a basic introduction to adaptive control theory and the design and simulation of two

different adaptive controller approaches, along with simulation results under different operational conditions of the system, will be presented. A comparison with simulation results obtained from classical control approaches will also be presented.

THIS PAGE INTENTIONALLY LEFT BLANK

## **IV. ADAPTIVE CONTROL**

### **A. INTRODUCTION**

According to Webster's dictionary, the definition of adapt is "to change (oneself) so that one's behavior will conform to new or changed circumstances" [22]. According to another definition, an adaptive system is any physical system that has been designed with an adaptive viewpoint [23]. From the above expressions, one can say that an adaptive controller is a controller that has the ability to change its behavior to adapt to changes in the systems dynamics. That means that to be adaptive, the controller has to have adjustable parameters.

Research on adaptive control systems was introduced during the 1950s, mostly for the design of high performance flight control systems. For many years, there has been skepticism among scientists about the use of adaptive control, since, in spite of the fact that the adaptation feature sounds very attractive, its performance and reliability may be questionable. In particular, when one applies it to a dynamic system, the designer should be aware that adaptation adds another loop, which might make the overall system unstable. Some important issues are the following [29]:

- Because of internal modulation effects, fast adaptation produces a high frequency input. This input excites unmodeled dynamics easily and causes systematic instability. Typical examples from [30] have shown that under very mild conditions of unmodeled dynamics, an adaptive control system can easily become unstable.
- There is no guarantee of the performance of the closed loop system during the transient response.

In the last few years, new applications of adaptive control have started to appear, and some of these issues have been addressed with a degree of success [31].

An adaptive control system can be thought as having two loops. One loop is a normal feedback loop, with the process and the controller. The second is the parameter adjustment loop.

The system is modeled in terms of a vector of parameters  $\theta$  that may be known or approximately known. The goal of the controller is to continuously produce a vector of estimates for the above parameters  $\tilde{\theta}$  and control the output vector.

## B. ADAPTIVE CONTROL THEORY

There are many different approaches to adaptive control. The model reference adaptive control (MRAC) and, more specifically, the direct MRAC (DMRAC), is used in this thesis. In this control scheme, the system is modeled in terms of a vector of parameters  $\theta_c$  that may be known or approximately known. This parameter vector is updated by an adaptive law using input and output data. A general view of the direct MRAC is shown in Figure 20.

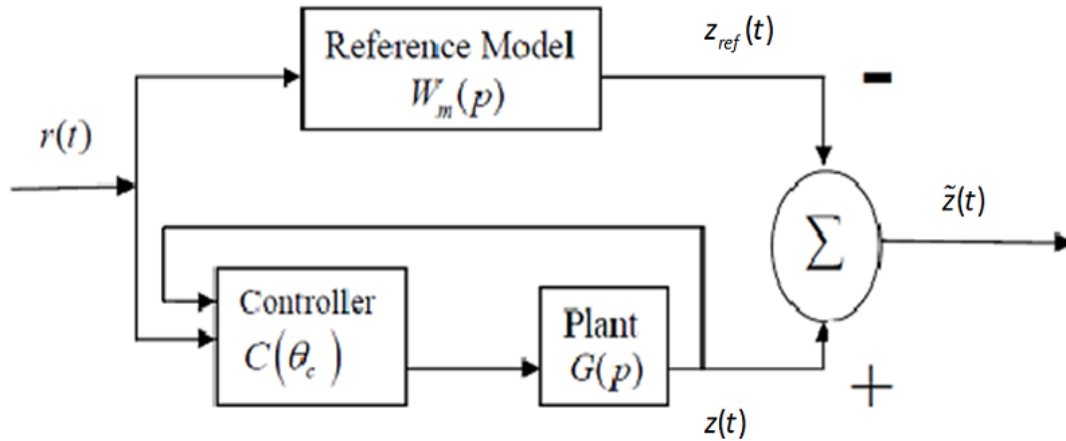


Figure 20. Direct MRAC overview. After [31].

As shown in Figure 20, the output of the system  $z(t)$  is compared to the output of a reference model  $z_{ref}(t)$ . The reference model is chosen to generate the desired trajectory for the plant output to follow [22]. The controller parameters are updated continuously, depending on the output error:

$$\tilde{z}(t) = z(t) - z_{ref}(t). \quad (0.0)$$

The goal of the controller is to continuously estimate the parameters giving a vector  $\hat{\theta}(t)$  to drive the error of the output vector  $\tilde{z}(t)$  to zero. The rest of this chapter examines the application of this to the dynamic model of the DFIG.

### C. ADAPTIVE CONTROL OF DFIG

Designing a control scheme required the evaluation of two different control approaches according to which part of the system should be adaptive:

- First approach: adaptive control of torque and reactive power using as output the rotor currents  $i_{qr}$  and  $i_{dr}$ .
- Second approach: adaptive control of torque and PI control of the reactive power using as output the rotor currents  $i_{qr}$  and  $i_{dr}$ .

These approaches are described in the following sections and the results obtained from simulation are discussed.

#### 1. First Approach: Adaptive Control for Torque and Reactive Power

In this approach, the controller was designed using adaptive control for both rotor currents components,  $i_{qr}$  and  $i_{dr}$ , which form the  $z(t)$  vector. The overall design is described in the following section.

##### a. Dynamic Model

The voltage equations of a DFIG expressed in an arbitrary chosen qd0 reference frame were described in Chapter II.

For the purposes of this design, one should assume that the reference frame is determined by the line voltage of the stator. In this frame, the stator voltage is a constant with value:

$$v_s(t) = v_{qs}(t) - jv_{ds}(t) = jV_s. \quad (0.0)$$



In addition, one can assume the stator resistance to be negligible; i.e.,

$$r_s = 0. \quad (0.0)$$

Then, defining the rotational frequency of the frame  $\omega$  to be the same as the electrical rotational frequency of the stator  $\omega_e$ , one can write Equation (2.28) as:

$$p\lambda_s = -j\omega\lambda_{dqs} + jV_s. \quad (0.0)$$

The solution of Equation (4.4), if the initial condition is  $\lambda_s(0) = \frac{V_s}{\omega}$ , is a constant given by

$$\lambda_s(t) = \frac{V_s}{\omega}. \quad (0.0)$$

Since the flux is complex  $\lambda_s(t) = \lambda_{qs}(t) - j\lambda_{ds}(t)$ , this yields

$$\begin{aligned} \lambda_{qs}(t) &= \frac{V_s}{\omega}, \text{ constant} \\ \lambda_{ds}(t) &= 0 \end{aligned} \quad (0.0)$$

The fact that the flux is a constant in this reference frame leads to the definition of a constant magnetizing current  $i_{ms}$ . The goal of the rest of this section is to rewrite the dynamic model of the DFIG in terms of the rotor current components  $i_{qr}$  and  $i_{dr}$  and the magnetizing current  $i_{ms}$  only.

Therefore, using Equations (2.31) from Chapter II relating the fluxes with the currents, one can obtain:

$$\begin{bmatrix} \lambda_s \\ \lambda'_r \end{bmatrix} = \begin{bmatrix} L_{ls} + L_M & L_M \\ L_M & L'_{lr} + L_M \end{bmatrix} \begin{bmatrix} i_s \\ i'_r \end{bmatrix}. \quad (0.0)$$

Substituting Equations (4.6) in (4.7), one gets:

$$\begin{aligned}(L_{ls} + L_M)i_{qs} + L_M i'_{qr} &= \frac{V_s}{\omega} . \\ (L_{ls} + L_M)i_{ds} + L_M i'_{dr} &= 0\end{aligned}\tag{0.0}$$

Solving Equation (4.8b) for  $i_{ds}$ , one gets:

$$i_{ds} = -\frac{L_M}{L_{ls} + L_M} i'_{dr} .\tag{0.0}$$

Now defining the constant magnetizing current  $i_{ms}$  as

$$L_M i_{ms} = \lambda_{qs} \Rightarrow i_{ms} = \frac{\lambda_{qs}}{L_M} \Rightarrow i_{ms} = \frac{V_s}{\omega L_M} ,\tag{0.0}$$

and substituting Equation (4.10) in Equation (4.8a) and solving for  $i_{qs}$ , one obtains:

$$\begin{aligned}L_M i_{ms} &= \frac{V_s}{\omega} \Rightarrow (L_{ls} + L_M)i_{qs} + L_M i'_{qr} \Rightarrow \\ i_{qs} &= \frac{L_M}{L_{ls} + L_M} i_{ms} - \frac{L_M}{L_{ls} + L_M} i'_{qr} .\end{aligned}\tag{0.0}$$

Now one can easily rewrite all the equations in terms of  $i_{ms}$  and  $i'_r$ . Substituting Equations (4.9), (4.10) and (4.11) in Equations (4.7) and expanding the expressions for  $\lambda_{qr}$  and  $\lambda_{dr}$ , one obtains:

$$\begin{aligned}\lambda_{qr} &= L_M i_{qs} + (L_{lr} + L_M) i'_{qr} \Rightarrow \\ \lambda_{qr} &= L_M \left( \frac{L_M}{L_{ls} + L_M} i_{ms} - \frac{L_M}{L_{ls} + L_M} i'_{qr} \right) + (L_{lr} + L_M) i'_{qr} \Rightarrow \\ \lambda_{qr} &= \frac{L_M^2}{L_{ls} + L_M} i_{ms} + \left( 1 - \frac{L_M^2}{(L_{ls} + L_M)(L_{lr} + L_M)} \right) (L_{lr} + L_M) i'_{qr}\end{aligned}\tag{0.0}$$

and

$$\begin{aligned}\lambda_{dr} &= L_M i_{ds} + (L_{lr} + L_M) i'_{dr} \Rightarrow \\ \lambda_{dr} &= L_M \left( -\frac{L_M}{L_{ls} + L_M} i'_{dr} \right) + (L_{lr} + L_M) i'_{dr} \Rightarrow \\ \lambda_{dr} &= \left( 1 - \frac{L_M^2}{(L_{ls} + L_M)(L_{lr} + L_M)} \right) (L_{lr} + L_M) i'_{dr}\end{aligned}\tag{0.0}$$

The flux linkages equations can then be summarized from Equations (4.6), (4.12) and (4.13) as:

$$\begin{aligned}\lambda_{qs} &= \frac{V_s}{\omega} \\ \lambda_{ds} &= 0 \\ \lambda_{qr} &= \frac{L_M^2}{L_{ls} + L_M} i_{ms} + \sigma(L_{lr} + L_M) i'_{qr} \\ \lambda_{dr} &= \sigma(L_{lr} + L_M) i_{dr}\end{aligned}\quad (0.0)$$

where  $\sigma$  is defined as a real parameter given by the following expression:

$$\sigma = 1 - \frac{L_M^2}{(L_{ls} + L_M)(L_{lr} + L_M)}, 0 < \sigma < 1. \quad (0.0)$$

In most cases,  $L_M$  is significantly larger than  $L_{ls}$  and  $L_{lr}$ , which means that  $\sigma$  is very small.

From Equations (2.28) in Chapter II, after ignoring the 0 components, which are negligible and defining

$$\omega - \omega_r = \tilde{\omega}, \quad (0.0)$$

one gets:

$$\begin{aligned}p\lambda_{qr} &= -r_r i_{qr} - \tilde{\omega} \lambda_{dr} + v_{qr} \\ p\lambda_{dr} &= -r_r i_{qr} + \tilde{\omega} \lambda_{qr} + v_{dr}\end{aligned}\quad (0.0)$$

Substituting Equations (4.14) in Equations (4.17), one finally obtains the desired dynamic model of DFIG in terms of magnetizing and the rotor currents:

$$\begin{aligned}pi_{qr} &= -\frac{r_r}{\sigma(L_r + L_M)} i_{qr} - \tilde{\omega} i'_{dr} + \frac{1}{\sigma(L_r + L_M)} v_{qr} \\ pi_{dr} &= -\frac{r_r}{\sigma(L_r + L_M)} i_{dr} + \tilde{\omega} i_{qr} + \tilde{\omega} \frac{L_M^2}{\sigma(L_r + L_M)(L_s + L_M)} i_{ms} + \frac{1}{\sigma(L_r + L_M)} v_{dr}\end{aligned}\quad (0.0)$$

Now, define  $\alpha_0, \alpha_l, b$  the following parameters:

$$\begin{aligned}
a_0 &= -\frac{r_r}{\sigma(L_r + L_M)} \\
a_1 &= \frac{L_M^2}{\sigma(L_r + L_M)(L_s + L_M)} i_{ms} \cdot \\
b &= \frac{1}{\sigma(L_r + L_M)}
\end{aligned} \tag{0.0}$$

Substituting Equations (4.19) in Equations (4.18), one ends up with two simple first order models:

$$\begin{aligned}
p i_{qr} &= a_0 i_{qr} - \tilde{\omega} i'_{dr} + b v_{qr} \\
p i_{dr} &= a_0 i_{dr} + \tilde{\omega} i_{qr} + \tilde{\omega} a_1 + b v_{dr} \cdot
\end{aligned} \tag{0.0}$$

By defining the state vector  $\underline{z} = \begin{bmatrix} i_{qr} \\ i_{dr} \end{bmatrix}$  and the control vector  $\underline{v} = \begin{bmatrix} v_{qr} \\ v_{dr} \end{bmatrix}$  and choosing two arbitrary positive constants  $\alpha_m, \beta_m$ , one can rewrite Equations (4.20) in terms of the state vector and a desired dynamic model:

$$\dot{\underline{z}}(t) = -\alpha_m \underline{z}(t) + \beta_m \underline{v}(t) + \Phi^T(t) \underline{\theta} + \tilde{\omega} \begin{bmatrix} -i_{dr} \\ i_{qr} \end{bmatrix}, \tag{0.0}$$

with

$$\Phi^T(t) = \begin{bmatrix} i_{qr} & 0 & v_{qr} \\ i_{dr} & \tilde{\omega} & v_{dr} \end{bmatrix} \tag{0.0}$$

$$\underline{\theta} = \begin{bmatrix} \alpha_0 + \alpha_m \\ \alpha_1 \\ b - \beta_m \end{bmatrix}$$

The significance of Equation (4.22) is that by defining the control signal as follows

$$\beta_m \underline{v}(t) = -\tilde{\omega}(t) \begin{bmatrix} -i_{dr} \\ i_{qr} \end{bmatrix} - \Phi^T(t) \hat{\underline{\theta}}(t) + \underline{W}_{ref}(t) \tag{0.0}$$

with  $\hat{\theta}(t)$  an estimate of the system parameter vector  $\theta(t)$ , the closed loop system becomes

$$\dot{\underline{z}}(t) = -\alpha_m \underline{z}(t) + \Phi^T(t) \tilde{\theta}(t) + \underline{W}_{ref}(t), \quad (0.0)$$

where

$$\tilde{\theta}(t) = \theta - \hat{\theta}(t). \quad (0.0)$$

In the ideal case of perfect knowledge of the DFIG dynamics, the parameter error vector  $\tilde{\theta}(t)$  in Equation (4.25) is zero, and the state vector  $z(t)$  tracks the reference model:

$$\dot{\underline{z}}_{ref}(t) = -\alpha_m \underline{z}_{ref}(t) + \underline{W}_{ref}(t). \quad (0.0)$$

The tracking error  $\tilde{z}(t)$  is defined as:

$$\tilde{z}(t) = z(t) - z_{ref}(t). \quad (0.0)$$

Then, combining Equations (4.24) and (4.26) and substituting in Equation (4.27), one ends up with the following expression:

$$\dot{\underline{z}}(t) = -\alpha_m \underline{z}(t) + \Phi^T(t) \tilde{\theta}(t). \quad (0.0)$$

Now, estimating the controller parameters requires the development of a differential equation, called the update law. That differential equation is of the form:

$$\dot{\tilde{\theta}}(t) = F\{y(t), e(t), \tilde{\theta}(t), \Phi(t)\}. \quad (0.0)$$

Using the steepest descent algorithm, we ensure that the parameter error decreases monotonically with time. In particular the definition of  $\dot{\hat{\theta}}(t)$  is as follows:

$$\dot{\hat{\theta}}(t) = \mu \Phi(t) \tilde{z}(t), \quad (0.0)$$

where  $\mu > 0$  is the adaptation gain of the controller. The definition of the following Lyapunov function is:

$$V(\theta, t) = \frac{1}{2} \|\tilde{z}(t)\|^2 + \frac{1}{2\mu} \|\tilde{\theta}(t)\|^2. \quad (0.0)$$

As also stated in Chapter III, for the system to be stable, the Lyapunov function described in Equation (4.31) has to be positive definite, and its derivative with respect to time must be negative semi-definite. By definition, it is positive definite, since in this case the parameters are positive real numbers and the norm of the parameter vectors are used. The derivative with respect to time of  $V(\theta(t))$  is

$$\dot{V}(\theta(t)) = \tilde{z}^T(t) \dot{\tilde{z}}(t) + \frac{1}{\mu} \tilde{\theta}^T(t) \dot{\tilde{\theta}}(t), \quad (0.0)$$

where, since  $\dot{\theta}(t) \approx 0$ , one can use the fact that:

$$\dot{\theta}(t) = -\dot{\tilde{\theta}}(t). \quad (0.0)$$

In Equation (4.32), if one substitutes Equations (4.28) and (4.30), one gets:

$$\dot{V}(\theta, t) = \tilde{z}^T(t) (-\alpha_m \tilde{z}(t) + \Phi^T(t) \tilde{\theta}(t)) - (\Phi(t) \tilde{z}(t))^T \tilde{\theta}(t) = -\alpha_m \|\tilde{z}(t)\|^2. \quad (0.0)$$

From Equation (4.34),  $\dot{V}(\theta, t)$  is negative semi-definite for every value of time  $t$ .

Equation (4.34) implies that:

$$V(t) \leq V(0) \forall t$$

$$\frac{1}{2} \|\tilde{z}(t)\|^2 + \frac{1}{2\mu} \|\tilde{\theta}(t)\|^2 \leq \frac{1}{2} \|\tilde{z}(0)\|^2 + \frac{1}{2\mu} \|\tilde{\theta}(0)\|^2, \quad (0.0)$$

which means, that if one chooses

$$\hat{z}(0) = z(0) \Rightarrow \tilde{z}(0) = 0, \quad (0.0)$$

And from Equation (4.35)

$$\|\tilde{z}(t)\| \leq \frac{\|\tilde{\theta}(0)\|}{\sqrt{\mu}}. \quad (0.0)$$

Equation (4.37) means that  $\tilde{z}(t)$  is bounded.

### b. Simulation Model

A Simulink model for the controller was created using the above equations for the system. The inputs to the controller are the following quantities, all expressed in the abc reference frame: stator voltages  $V_{abc}$ , stator and rotor currents  $i_{abc}$  and  $i_{abc}$  respectively,  $\omega_r$  and the reference currents  $i_{qr\_ref}$  and  $i_{dr\_ref}$ . The outputs of the controller are the rotor voltages that go into the DFIG model. A general block diagram of the controller is shown in Figure 21.

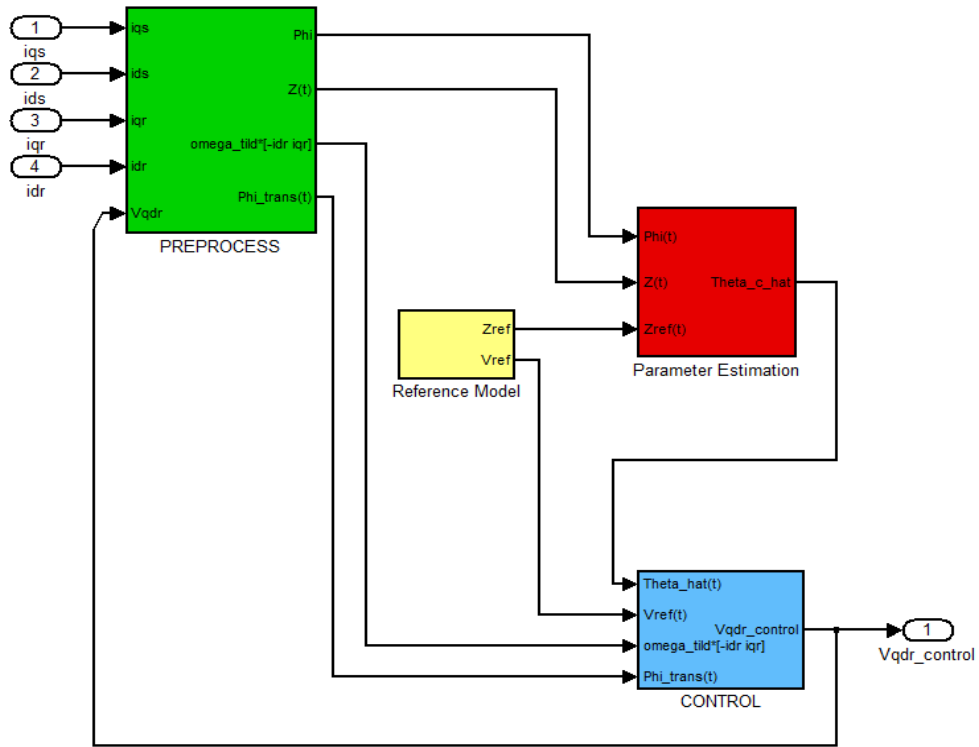


Figure 21. General view of the first controller in Simulink.

This model was created using Equations (4.18) to (4.37). A detailed view of the controller block, which gives the values of the control vector  $\begin{bmatrix} v_{qr} & v_{dr} \end{bmatrix}^T$  according to Equation (4.23), is shown in Figure 22. The output is then transformed back to the  $abc$  reference frame to supply the rotor with the proper control voltage.

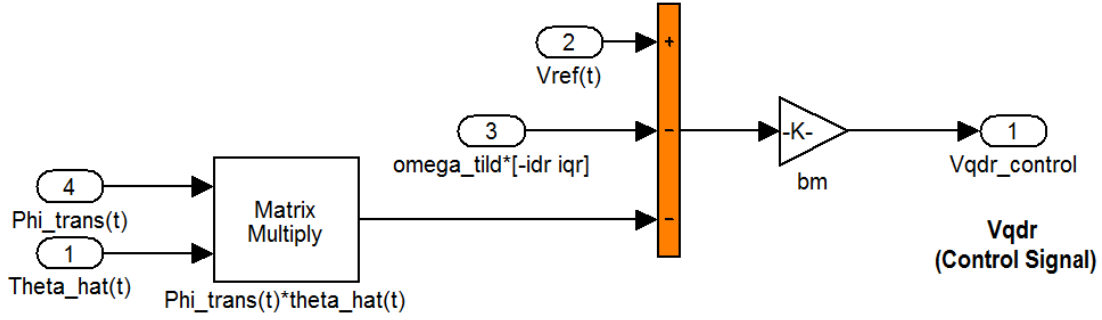


Figure 22. Control block for the first approach.

The reference model shown in Figure 21 has a first order transfer function of the form

$$T(s) = \frac{a_m}{s + a_m} \quad (0.0)$$

The control goal is to independently control the rotor currents to minimize the reactive power of the DFIG and to produce the maximum real power for every different value of the wind speed respectively.

From Equation (2.36), after substituting the values of  $V_{qs}$  and  $V_{ds}$  from Equation (4.2), one can obtain the following expression for the reactive power:

$$Q_e = -\frac{3}{2} V_s i_{qs} \quad (0.0)$$

which means that  $Q_e$  is proportional to  $i_{qs}$ , so to have  $Q_e = 0$ ,  $i_{qs}$  has to be equal to zero; i.e.,



$$i_{qs\_ref} = 0 . \quad (0.0)$$

From equation (4.11), substituting the above value for  $i_{qs\_ref}$  from Equation (4.40), one gets:

$$I_{qr\_ref} = i_{ms} , \quad (0.0)$$

which means that  $i_{qr}$  should be equal to the magnetizing current, which is constant after the system reaches steady-state, and is given by Equation (4.10).

On the other hand, keeping the power output maximum requires that the electric torque of the DFIG be equal to the aerodynamic torque that gives the maximum power output of the WT for each wind speed, which is given by [12]

$$T_{e\_ref} = T_{aero\_optimal} = K_{opt} \Omega_r^2 , \quad (0.0)$$

where

$$K_{opt} = \frac{1}{2} \rho \pi R^5 \frac{C_p(\lambda_{opt})}{\lambda_{opt}^3} \quad (0.0)$$

and  $\Omega_r$  is the rotational speed of the WT in revolutions per minute (RPM). This is given by

$$\Omega_r = \frac{1}{Gear\_Ratio P} \omega_r , \quad (0.0)$$

where  $Gear\_Ratio$  is the gear box ratio,  $P$  is the number of poles of the DFIG, and  $\omega_r$  is the electrical rotational speed of the rotor in radians per second.

The expression of the electric torque output of the DFIG is given by Equation (2.35). Substituting the values of the flux linkages from Equation (4.6), one gets

$$T_e = -\left(\frac{3}{2}\right)\left(\frac{P}{2}\right)L_M\left(\frac{V_s}{\omega_b} i_{ds}\right) , \quad (0.0)$$

and by substituting  $i_{ds}$  from Equation (4.9) into Equation (4.45), one obtains

$$T_e = -\left(\frac{3}{2}\right)\left(\frac{P}{2}\right)L_M \frac{V_s}{\omega_b} \left(-\frac{L_M}{L_s + L_M} i_{dr}\right). \quad (0.0)$$

The goal is to track a reference torque, which requires  $T_e = T_{e\_ref}$ . That means that from Equations (4.44) and (4.46) one should set the reference current  $i_{dr}$  that is driving the reference model to be

$$i_{dr\_ref} = \frac{T_{e\_ref}}{\left(\frac{3}{2}\right)\left(\frac{P}{2}\right)L_M \frac{L_M}{L_s + L_M} \frac{V_s}{\omega_b}}. \quad (0.0)$$

Running the model required the inclusion of a block that takes the current wind speed as input and gives the instant aerodynamic torque as output, which is the excitation of the DFIG. The WT turbine speed is then given by

$$J\dot{\Omega}_r = T_{aero} - T_e, \quad (0.0)$$

where  $J$  is the combined inertia of the WT and the DFIG rotor. In this thesis, the rotor inertia was neglected due to its very small value compared to the inertia of the WT.

The comparison of the control approaches presented here with other controllers required the use of the parameters of the DFIG and the WT described in [7], which are shown in Table 3.

Table 3. WT and DFIG parameters. From [7].

<i>Wind Turbine</i>	<i>DFIG</i>
$R = 3.8 \text{ m}$	$P_{max} = 50 \text{ hp} = 37.285 \text{ kW}$
$J = 3.362 \text{ kgm}^2$	$P = 4$
$a = 19.346$	$R_s = 0.082$
$b = 9.4117$	$R_r = 0.228$
$c = 20$	$L_s = 0.0355 \text{ Hy}$
$\text{Gear\_Ratio } 16:1$	$L_r = 0.0355 \text{ Hy}$
$\lambda_{opt} = 6.4$	$L_M = 0.0347 \text{ Hy}$
	$\omega_{b\_} = 2\pi 60 \text{ rad/s}$
	$V_s = 380 \text{ V}$

*c. Simulation Results*

After a large number of simulations, the system parameters that gave the best results are shown in Table 4. The sampling time for the simulation was chosen equal to 0.8 ms. For these values, the system was stable and tracked the reference model for wind speeds from 3.2 m/s to 10.8 m/s, which is a good range. This covered almost all the operational range of the WT.

Table 4. Final simulation parameter values for first approach.

<i>Parameter</i>	<i>Value</i>
$a_m$	100
$b_m$	250
$\mu_{11}$	0.75
$\mu_{22}$	50
$\mu_{33}$	0.4

In Table 4, it can be seen that the adaptation gain for the parameter estimation was chosen to be a diagonal matrix as seen in Chapter III to improve the convergence of the estimates. The initial condition for the estimates was chosen equal to 70% of the expected values calculated using Equation (4.22).

The wind speed profile used is shown in Figure 23 along with a plot of the absolute values of the actual output torque  $T_e$  and the reference torque  $T_{ref}$ . The wind speed profile was chosen in order to prove the performance of the controller even for large rapid changes in wind speed, greater than 5 m/s, which can be considered wind gusts according to [33].

The output torque is tracking the reference value for a range of wind speeds from 3.2 m/s to 10.7 m/s as shown in Figure 23.

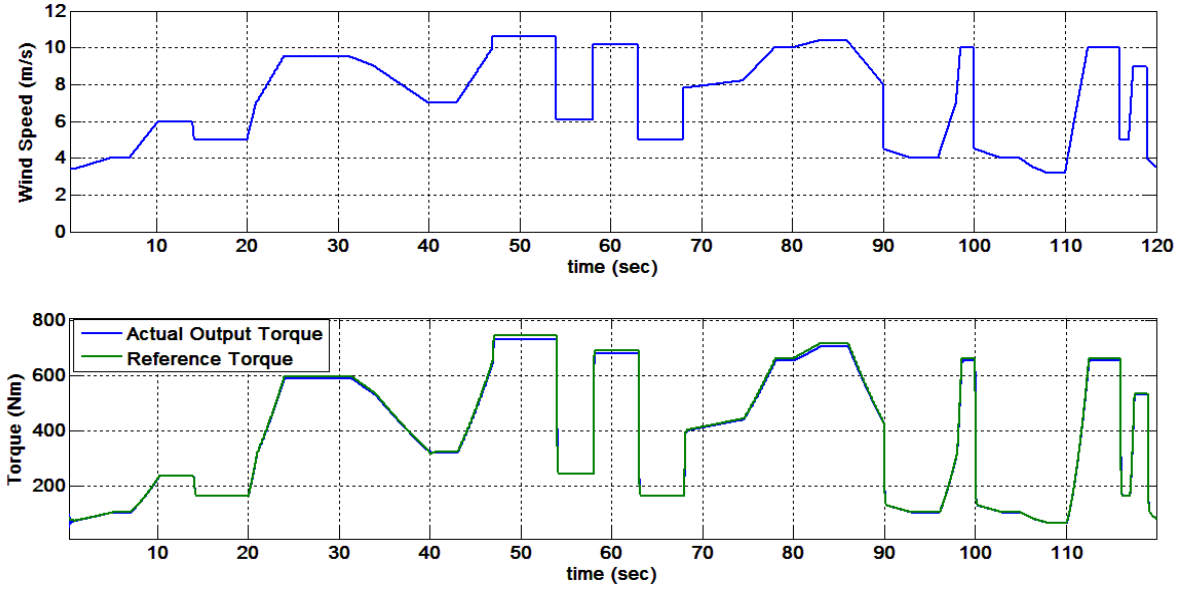


Figure 23. Wind speed and torque during simulation of the first approach.

Zooming in on the torque plot from time 90 s to 120 s in Figure 24, one can see that even for wind changes of 6.8 m/s, the difference between reference and actual output is less than 1.65 %. For lower wind speeds, the difference is always less than 0.7 %, which is a very satisfactory result.

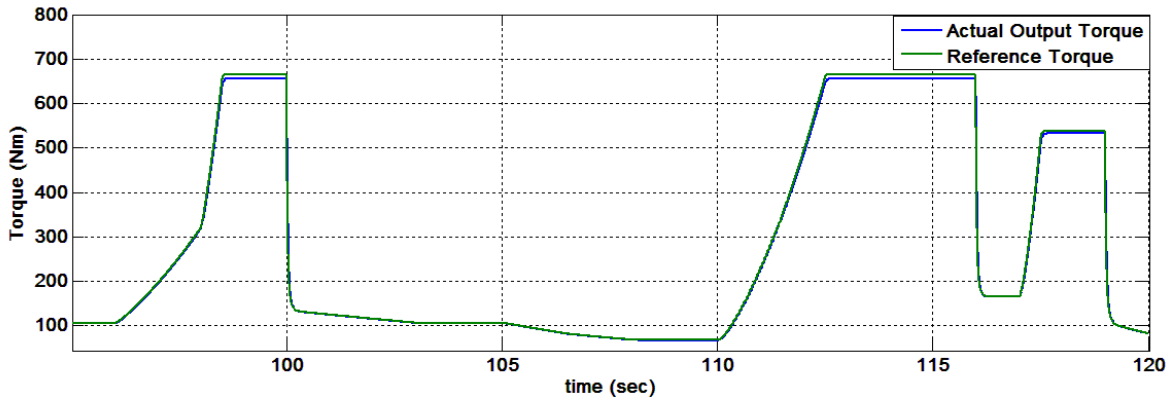


Figure 24. Magnified torque plot during simulation of the first approach.

The plots of the real power  $P_e$  and reactive power  $Q_e$  during the simulation are shown in Figures 25 and 26, respectively.

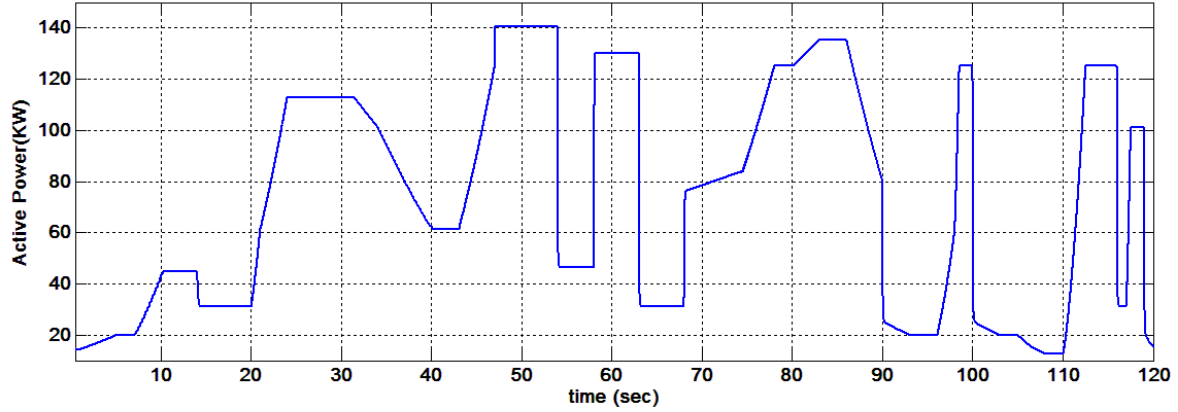


Figure 25. Real power ( $P_e$ ) during simulation of the first approach.

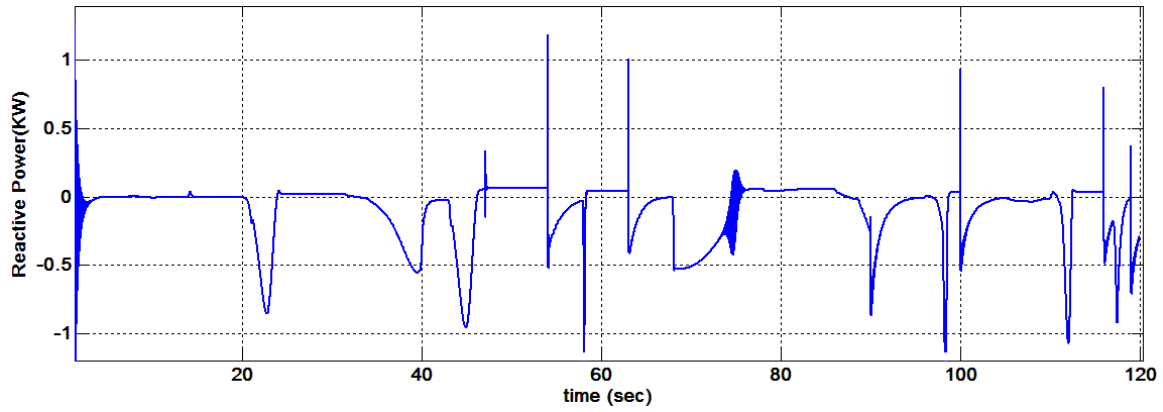


Figure 26. Reactive power ( $Q_e$ ) during simulation of the first approach.

In Figures 25 and 26, one can see that the ratio of  $Q_e$  over  $P_e$  is very small and remains less than 0.2% for most the simulation time. This result indicates that the second goal of the design is also satisfied. The only time that  $Q_e$  increases, but still with values less than 1% of  $P_e$ , is during extreme changes in wind speed, and that happens for a very short period.

The rotor currents during the simulation are shown in Figure 27.

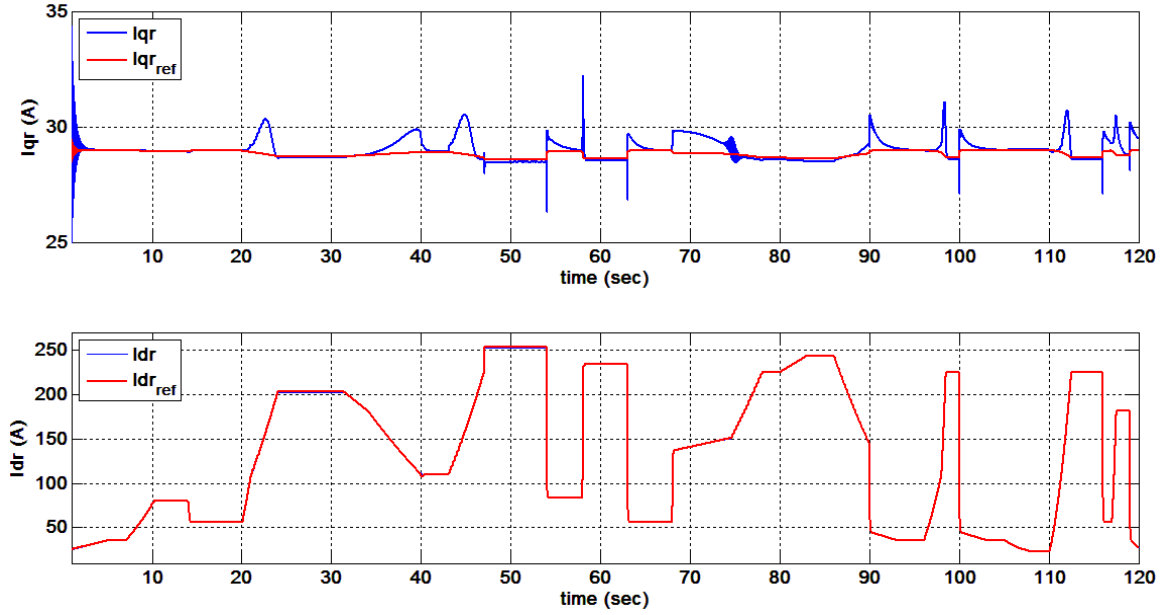


Figure 27. Comparison of the rotor currents  $i_{qr}$  and  $i_{dr}$  with their reference values during simulation of the first approach.

## 2. Second Approach: Adaptive Control of Torque, PI Control of the Reactive Power

A second approach was attempted to simplify the controller with only one adaptive loop for torque control. The difference in this approach is that instead of controlling both  $i_{qs}$  and  $i_{dr}$  adaptively, a PI controller was used for  $i_{qs}$  and the adaptive control for  $i_{dr}$  was kept.

### a. Dynamic Model of the Controller

Equations (4.2) to (4.18) are valid for this approach. From Equation (4.11), solving for  $i_{qr}$ , one gets

$$i_{qr} = i_{ms} - \frac{L_M + L_{ls}}{L_M} i_{qs}. \quad (0.0)$$

Substituting Equation (4.49) for the last one of Equations (4.18), one obtains

$$p i_{dr} = -\frac{r_r}{\sigma(L_{lr} + L_M)} i_{dr} + \tilde{\omega} \left( i_{ms} - \frac{L_M + L_{ls}}{L_M} i_{qs} \right) + \tilde{\omega} \frac{L_M^2}{\sigma(L_{lr} + L_M)(L_{ls} + L_M)} i_{ms} + \frac{1}{\sigma(L_{lr} + L_M)} v_{dr} . \quad (0.0)$$

$$p i_{dr} = -\frac{r_r}{\sigma(L_{lr} + L_M)} i_{dr} - \tilde{\omega} \left( \frac{L_M + L_{ls}}{L_M} \right) i_{qs} + \tilde{\omega} \left( 1 - \frac{L_M^2}{\sigma(L_{lr} + L_M)(L_{ls} + L_M)} \right) i_{ms} + \frac{1}{\sigma(L_{lr} + L_M)} v_{dr}$$

One defines the following parameters:

$$\begin{aligned} a_0 &= -\frac{r_r}{\sigma(L_{lr} + L_M)} \\ a_1 &= \frac{L_{ls} + L_M}{L_M} \\ a_2 &= \left( 1 - \frac{L_M^2}{\sigma(L_{lr} + L_M)(L_{ls} + L_M)} \right) i_{ms} \\ b &= \frac{1}{\sigma(L_{lr} + L_M)} \end{aligned} \quad (0.0)$$

Substituting Equations (4.51) in Equation (4.50), one gets

$$p i_{dr} = a_0 i_{dr} - a_1 (\tilde{\omega} i_{qs}) + a_2 \tilde{\omega} + b v_{dr} . \quad (0.0)$$

Now  $\underline{z}_r = i_{dr}$  and  $\underline{v} = v_{dr}$  are called the state and control signal, respectively, which in this approach are scalars. Then, for any arbitrary constant  $\alpha_m, \beta_m$  one can write Equation (4.52) in the form

$$\dot{\underline{z}}(t) = -\alpha_m \underline{z}(t) + \beta_m \underline{v}(t) + \Phi^T(t) \underline{\theta} . \quad (0.0)$$

where

$$\Phi^T(t) = \begin{bmatrix} i_{dr} & -\tilde{\omega} i_{qs} & \tilde{\omega} & v_{dr} \end{bmatrix} \quad (0.0)$$

and

$$\underline{\theta} = \begin{bmatrix} \alpha_0 + \alpha_m \\ a_1 \\ a_2 \\ b - \beta_m \end{bmatrix} . \quad (0.0)$$

In this case, the control signal is

$$\beta_m \underline{v}(t) = -\Phi^T(t) \hat{\underline{\theta}} + \underline{W}_{ref}(t). \quad (0.0)$$

Now substitute Equation (4.56) into Equation (4.53), and one gets:

$$\dot{\underline{z}}(t) = -\alpha_m \underline{z}(t) + \Phi^T(t) \tilde{\underline{\theta}}(t) + \underline{W}_{ref}(t), \quad (0.0)$$

where  $\tilde{\underline{\theta}}(t)$  is given by Equation (4.25).

### b. Simulation Model

The general view of the controller in Simulink is shown in Figure 28.

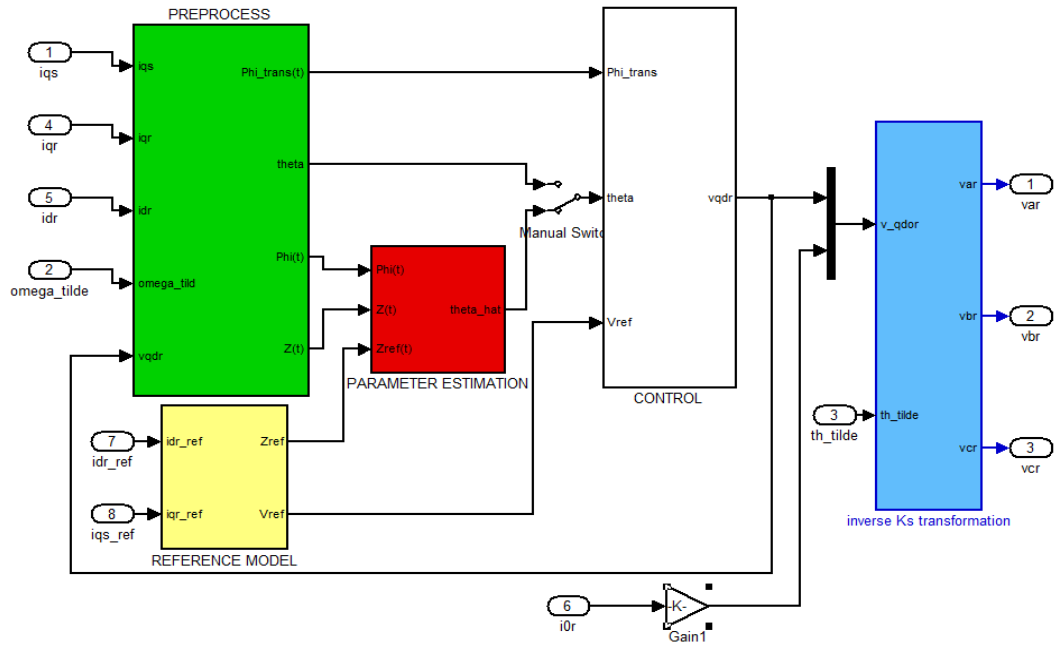


Figure 28. General view of the second controller model.

Equations (4.30) to (4.37), which were used in the first approach for the parameter estimates, were also used for this case.

For  $i_{qs}$ , a PI controller was used with the transfer function

$$T_{pi}(s) = \frac{K_1 s + K_0}{s}, \quad (0.0)$$



where  $K_0$ ,  $K_I$  are the gains of the PI controller. The input of this controller, the error between the reference and the actual measured value of  $i_{qs}$  and the output is  $v_{qr}$ .

Furthermore, Equations (4.42) to (4.48) that give the expression for  $i_{dr\_ref}$  and  $\Omega_r$  were again used here.

In this approach, the output of the adaptive controller is  $v_{dr}$  according to Equation (4.57); two low pass (LP) filters were added in the output of the adaptive part to filter higher frequency components that might affect the stability of the system. A detailed view of the control block diagram is shown in Figure 29.

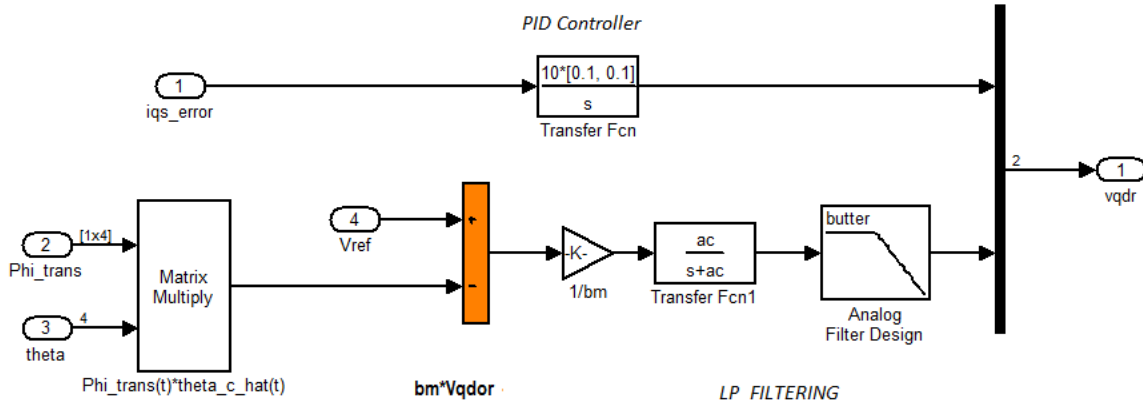


Figure 29. Control block for the second approach.

The cutoff frequency  $a_c$  in the LP filter shown in Figure 29 was 100, and for the second filter, which is a 12<sup>th</sup> order Butterworth filter, the cutoff frequency was 10 times higher.

### c. Simulation Results

After a large number of simulations, the system parameters that gave the best results for this approach are those shown in Table 5. The sampling time for the

simulation was equal to 0.8 ms. For these values, the system was stable and tracked the reference model for wind speeds from 3.2 m/s to 10.8 m/s.

Table 5. Final simulation parameter values for the second approach.

<i>Parameter</i>	<i>Value</i>
$a_m$	100
$b_m$	250
$\mu_{11}$	100

In Table 5, it can be seen that the adaptation gain for the parameter estimation in this case was a single value, which is about two orders of magnitude larger than the adaptation gains for the first approach given in Table 4. This value was chosen because comparable results could not be achieved between the two control approaches with smaller values of  $\mu$ . The initial condition for the estimates was chosen equal to 70% of the expected values calculated using Equations (4.56).

The wind speed profile is the same as the one used in the previous approach, which allows for a comparison between approaches in the next chapter. This plot, along with a plot of the absolute actual output torque  $T_e$  and the reference (optimal) torque  $T_{ref}$ , is shown in Figure 30.

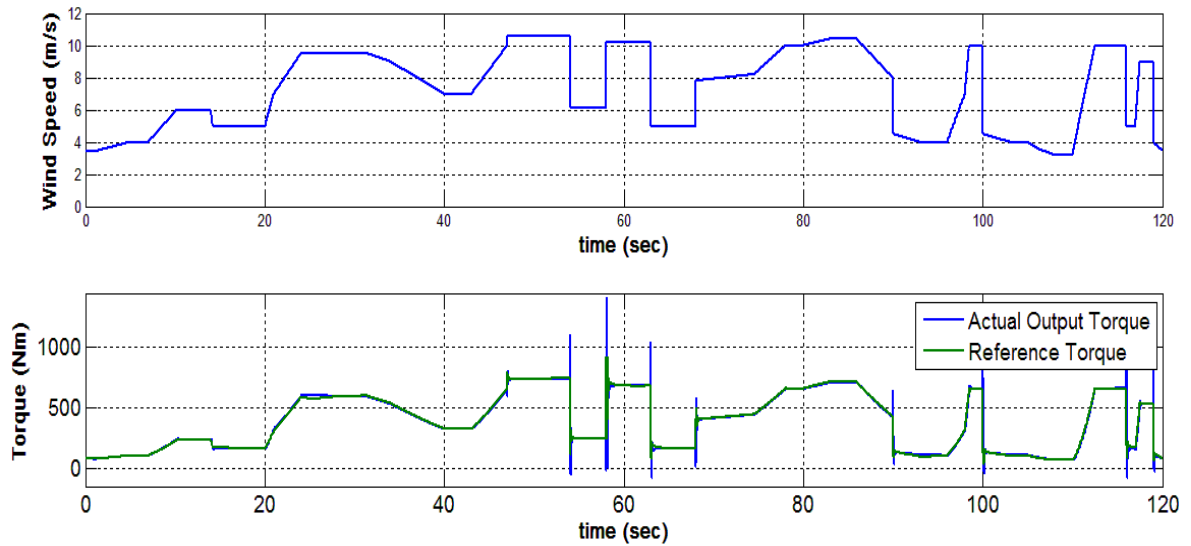


Figure 30. Wind speed and torque during simulation of the second approach.

From Figure 30, it can be seen that the output torque tracks the reference value pretty well for a range of wind speeds from 3.2 m/s to 10.7 m/s, but during the sudden wind changes, the actual output torque spikes for a few moments. A zoomed in view of the torque plot from time 97 s to 119 s is illustrated in Figure 31.

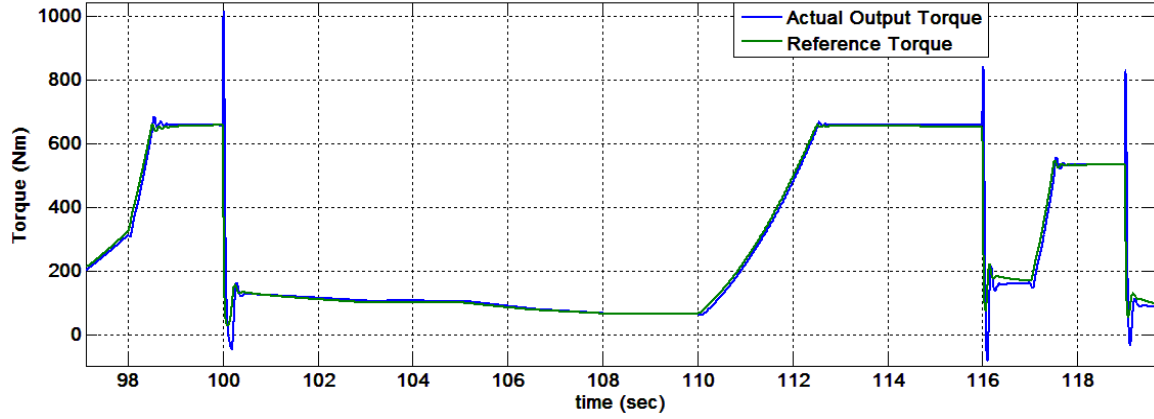


Figure 31. Magnified torque during simulation of the second approach.

It can be seen in Figure 31 that for large and fast wind changes that simulate wind gusts, the torque tends to lose tracking for few moments. This is especially true when the wind decreases, e.g. at 100 s or at 117 s of simulation time, where the difference between the two values even reaches 100% but recovers quickly.

The plots of the real power  $P_e$  and reactive power  $Q_e$  during the simulation of the second approach are shown in Figures 32 and 33, respectively.

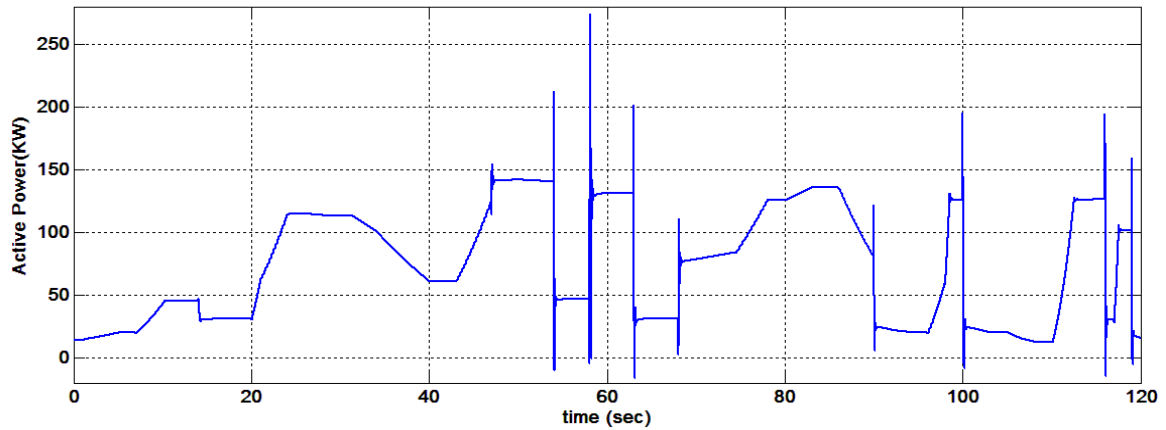


Figure 32. Real power ( $P_e$ ) during simulation of the second approach.

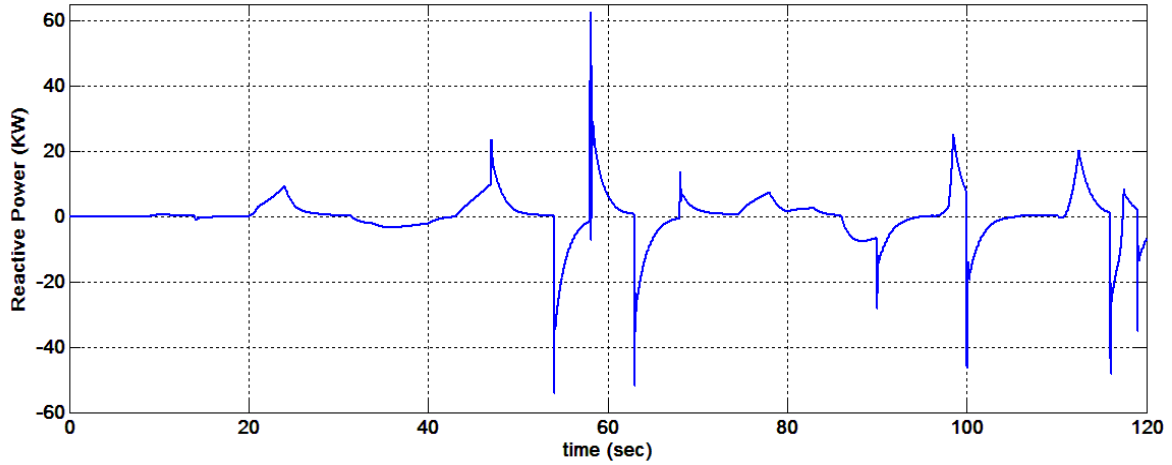


Figure 33. Reactive power ( $Q_e$ ) during simulation of the second approach.

It is can be seen in Figure 33 that  $Q_e$  is quite high compared to  $P_e$ . This is clearer if one zooms in on a part of the simulation, as shown in Figure 34.

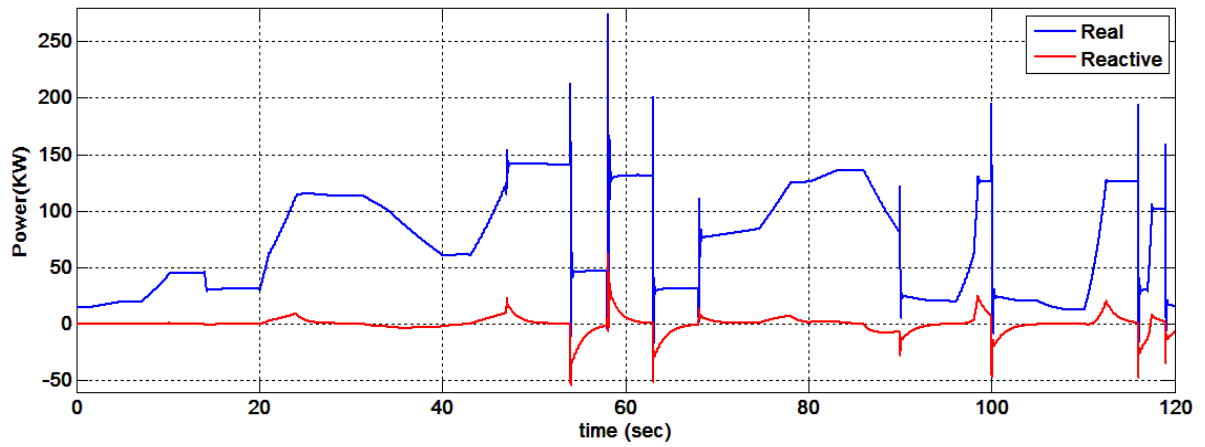


Figure 34. Comparison between real and reactive power  $P_e$  and  $Q_e$ , respectively, for part of the simulation during the second approach.

Finally, the plots of the currents  $i_{qs}$  and  $i_{dr}$  are shown in Figure 35.

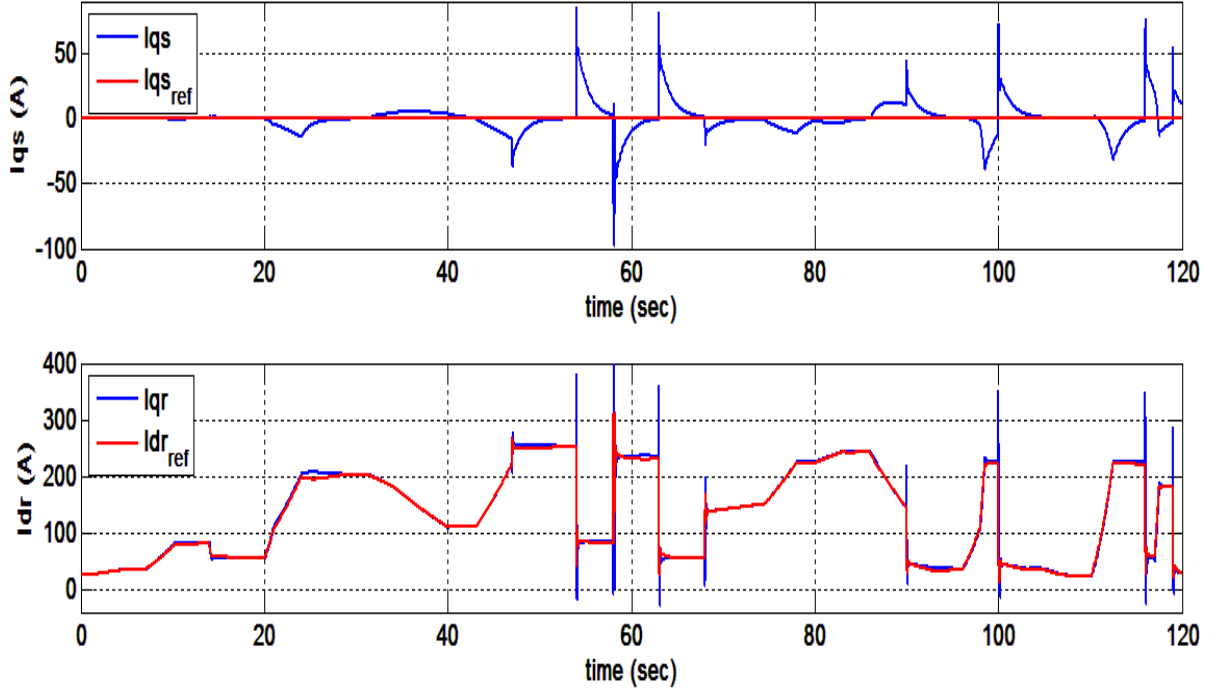


Figure 35. Comparison of the currents  $i_{qs}$  and  $i_{dr}$  with their reference values during simulation of the second approach.

It can be seen in Figure 35 that  $i_{dr}$  is tracking its reference value very well, but  $i_{qs}$  seems to lose tracking during sudden wind speed changes.

### 3. Performance Comparison

To be able to reach a conclusion on the performance of the controllers designed in this study, a Simulink model of a classical approach for the control of a WECS was created. This is described in [12], again using the parameters of the system given in [7]. The model was created for [33].

Two different fault cases were simulated to compare the robustness of the control algorithms. These two are:

- a wind gust, i.e., a sudden increase in the wind speed from 6 to 10 m/sec,
- doubling of the value of the rotor resistance  $r_r$  to demonstrate what happens during a parameter variation.

The wind profile shown in Figure 36 was assumed.

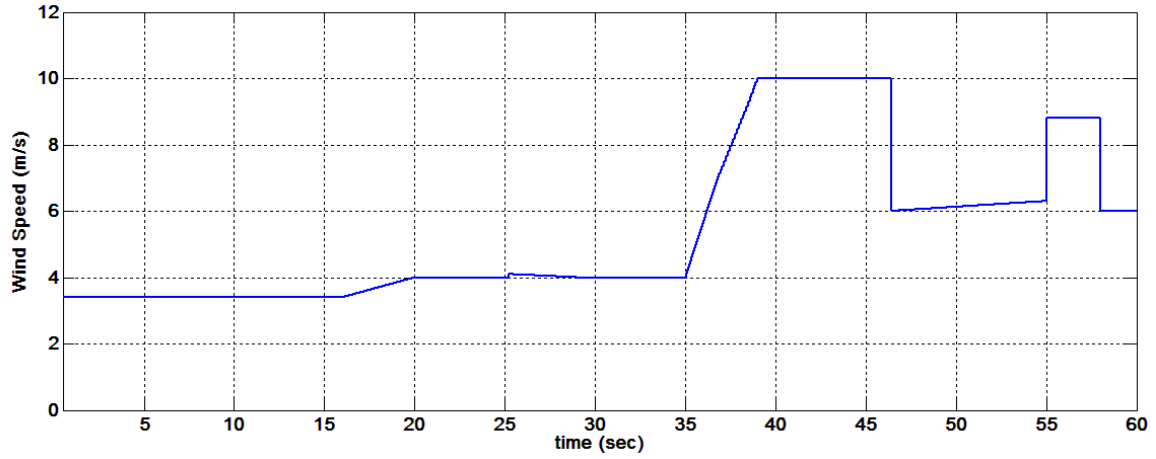


Figure 36. Wind profile for comparison of the control approaches.

The output torque of the three different control approaches during simulation is shown in Figure 37.

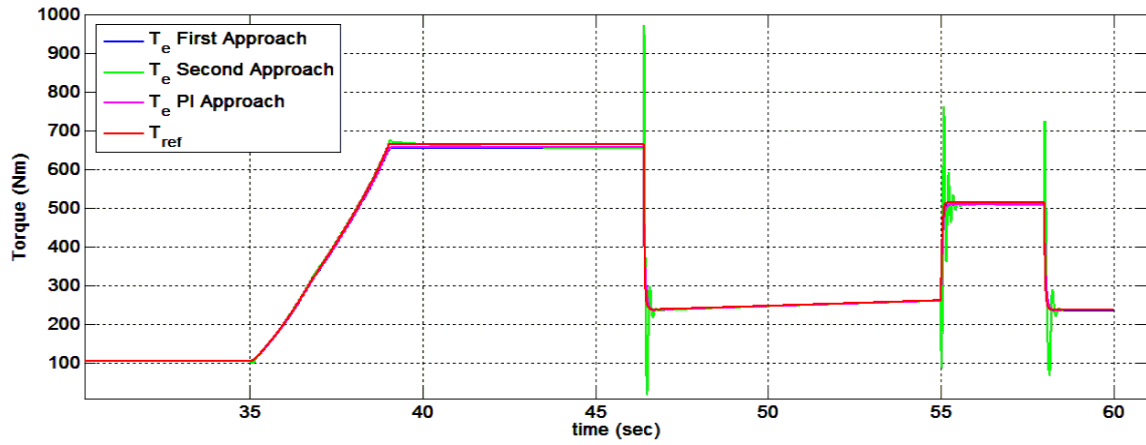


Figure 37. Comparison of output torque  $T_e$  and reference torque  $T_{ref}$  during the simulation of a wind gust.

Magnifying Figure 37 for about 10 s during the top of the wind gust provides Figure 38.

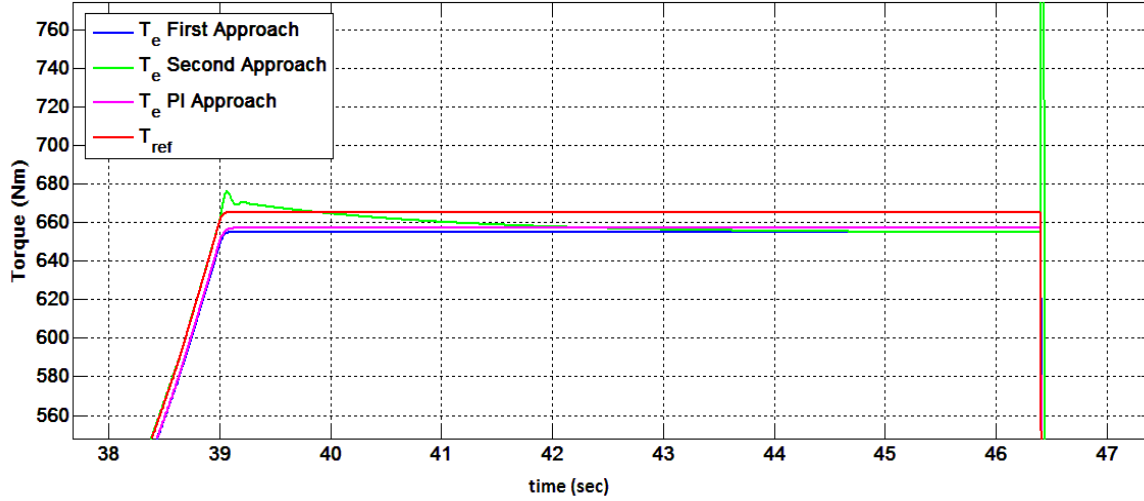


Figure 38. Magnified plot of output torque  $T_e$  and reference torque  $T_{ref}$  during the simulation of a wind gust.

From Figure 38, one can see that even though the performance of all the approaches considered is very good, the output torque of the first approach and the classical approach with the PI controllers are identical and almost identical, respectively, to the reference torque throughout the simulation, while the second approach shows some oscillation during sudden wind speed changes. Furthermore, the torque of the classical approach is slightly closer to the reference value, but has more overshoot compared to the first approach.

The resistance of the rotor is a parameter that affects the shape of the torque output of the DFIG [19] and is illustrated in Figure 39.

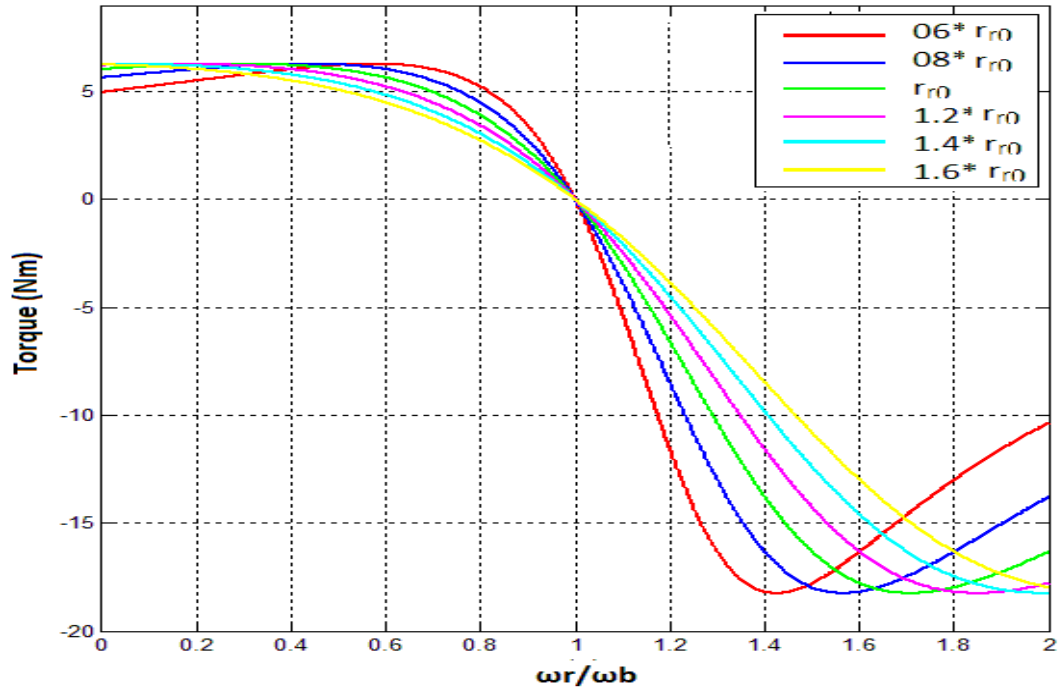


Figure 39. Typical DFIG torque versus time curve for different values of  $r_r$ .

For the purposes of this thesis, in order to investigate the performance of the controllers that we proposed in previous sections, the rotor's resistance  $r_r$  was increased to twice its initial value at  $t=15$  s of the simulation, and all the control approaches where simulated. The output torque plots during the above change in  $r_r$  from the simulations are shown in Figure 40.

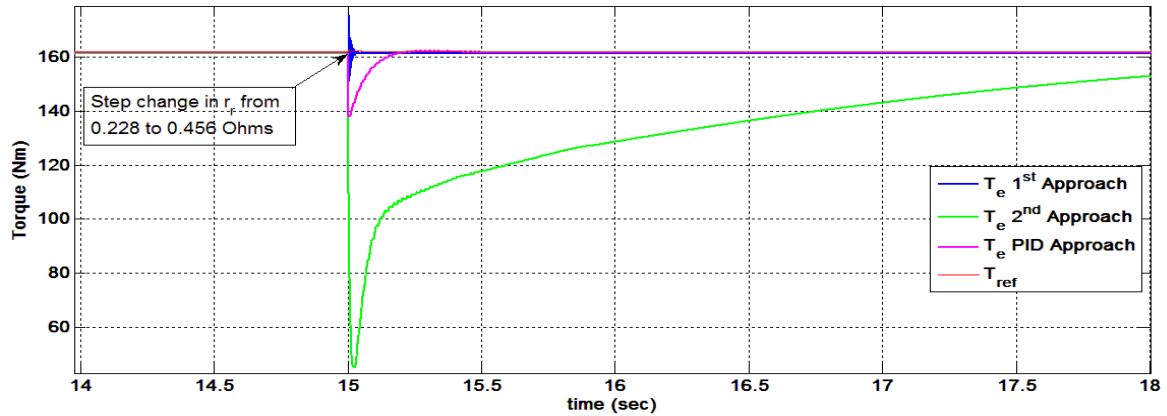


Figure 40. Comparison of the variation of the output torque curves during simulation of a variation of  $r_r$ .



As seen in Figure 40,  $T_e$  for the second approach has a high overshoot and even after three seconds does not completely track the reference torque  $T_{ref}$ . Between the other two cases, the first approach appears to have the best performance since it has a small spike in  $T_e$  but recovers faster than the PID approach. This can also be seen in Figure 41, where the speed of the DFIG for the three approaches is presented around the step change in  $r_r$ ; it is clear that the first adaptive approach gives the smoother speed curve among the three different cases.

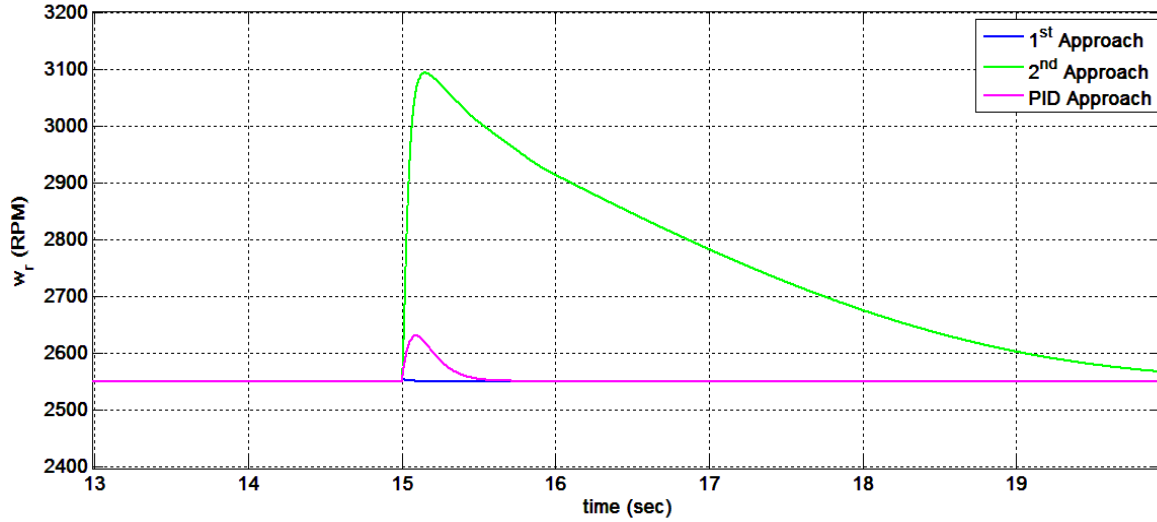


Figure 41. Comparison of the variation of the DFIG speed during the simulation of a variation of  $r_r$ .

#### D. CHAPTER SUMMARY

In this chapter, the analytical design, modeling and simulation of two MRAC approaches for a DFIG-based WECS were presented. The simulation results were compared with results from simulation of a more classical control approach for this kind of system, which was presented in [12]. The conclusions from these comparisons along with recommendations for future research are discussed in Chapter V.

## **V. CONCLUSIONS AND RECOMMENDATIONS**

### **A. SUMMARY - CONCLUSIONS**

The problem of the control of a doubly-fed induction generator based wind energy conversion system with fixed pitch horizontal axis wind turbine was addressed in this thesis. The adaptive control used was direct model reference adaptive control. This research effort addressed issues relative to the identification of the system's parameters and the design of adaptive control techniques in order to compensate for uncertain or time-varying dynamics.

In particular three system identification algorithms were presented based on standard techniques such as least mean squares (LMS) or recursive least squares (RLS) with and without exponential forgetting. The significance of these techniques is that a dynamic system of the DFIG can be properly parameterized on the basis of experimental results.

Furthermore, two different adaptive control approaches were introduced and simulated for application in wind power generation. In this case it turns out that the parameterized dynamic model, based on the magnetic fluxes of stator and rotor, can be simplified considerably and only a few parameters have to be estimated. This is due to the stator being connected to the grid so that the stator voltage is constant in magnitude, frequency and phase. Given this characteristic, the magnetizing current becomes one of the parameters to be estimated, which results in considerable simplification of the dynamic model.

These approaches have been tested in numerous simulations and seem to present an attractive solution to the problem of compensating for uncertain dynamics such as varying resistances and impedances in the circuitry.

## **B. RECOMMENDATIONS-FUTURE RESEARCH**

Extensive computer simulations demonstrate that the algorithms presented for adaptive control work as expected. Next step in this research will be the implementation of the proposed controllers in a laboratory environment using a direct current motor to simulate the wind turbine and building the controllers using Xilinx software in Simulink and field programmable gate arrays to establish bidirectional communication between the software and the equipment.

This effort will involve not only actual real-time implementation but also the design of an appropriate model for the wind profile so that wind effects can be simulated by the generation of appropriate torque by the DC motor. The ultimate benefit of this research will be more efficient wind power generators.

## APPENDIX: MATLAB CODES - SIMULINK MODEL

In this Appendix, the code that was used for the initialization of the simulations, as well as the basic block of the Simulink models for the controllers are presented.

### A. MATLAB CODE FOR INITIALIZATION OF THE SIMULATIONS

```
%% INITIAL CONDITIONS FILE

clc;
clear all;

omega_b = 2*pi*60;
tstep=.0005;
tstop=120;
twopi3 = 2*pi/3;
poles = 4;
J=3.362; % kg m^2
polesby2J = poles/2/J;

GearRatio=16;

%Parameters from paper on nonlinear control

rr0 =0.228; % ohms
rs=0.02; % ohms
Xls=omega_b*(0.0355-0.0347); % ohms
Xm =omega_b*0.0347; % ohms
Xlr =omega_b*(0.0355-0.0347); % ohms

Vs=380; % Volts Grid phase voltage
omega_e=omega_b; %electrical frequency

%Parameters - Equivalent circuit

Ls=Xls/omega_b;
Lm=Xm/omega_b;
Lr=Xlr/omega_b;
rsbyXls = rs/Xls;
rrbyXlr = rr0/Xlr;
Xaq = 1/(1/Xm+1/Xls+1/Xlr);
Xad = Xaq;
XaqbyXls = Xaq/Xls;
XaqbyXlr = Xaq/Xlr;
XadbyXls = Xad/Xls;
XadbyXlr = Xad/Xlr;
V_phase = 380*sqrt(2)/sqrt(3); %Peak value used in Simulink for source
model
```

```

%Steady state analysis
omegar_ic = omega_b*.85;
slip = 0.001; %start at synchronous speed
Z1 = rs + j*Xls;
Z2 = j*Xm;
Z3 = rr0/slip + j*Xlr;
Ias = V_phase/sqrt(2)/(Z1 + Z2*Z3/(Z2+Z3));
Iar = -Ias*(Z2*Z3/(Z2+Z3))/Z3;
Te = 3*poles/2*Xm/omega_b*real(j*conj(Ias)*Iar);
Iqse = sqrt(2)*real(Ias);
Idse = -sqrt(2)*imag(Ias);
Iqre = sqrt(2)*real(Iar);
Idre = -sqrt(2)*imag(Iar);
psi_mqe = Xm*(Iqse+Iqre);
psi_mde = Xm*(Idse+Idre);
psi_qse = Iqse*Xls + psi_mqe;
psi_dse = Idse*Xls + psi_mde;
psi_qre = Iqre*Xlr + psi_mqe;
psi_dre = Idre*Xlr + psi_mde;
psi_qsic=psi_qse;
psi_dsic=psi_dse;
psi_qric=psi_qre;
psi_dric=psi_dre;

%WIND
rho=1.225; % air density
lam=0.1:.1:10;
C=(19.346./lam).*(9.4117./lam -1).*exp(-20./lam);
% plot(lam, C)
lam_opt=6.4;
C_opt=C(64);
K_opt=rho*pi*(3.8^5)*C_opt/(2*lam_opt^2);
lamda=0.8;

%MRAC parameters
am=100.0; % this works
bm=250;

% Filter frequency
ac=500;

sigma=1-(Lm^2)/((Ls+Lm)*(Lr+Lm));
b=1/(sigma*(Lr+Lm));
a0=-rr/(sigma*(Lr+Lm));
c=50;

% controller parameters
im0=Vs/(omega_e*Lm); % estimated magnetizing current

% true values
theta(1)=a0+am;
theta(2)=Lm/(Ls+Lm);
theta(3)=-im0*a0*Lm/(Ls+Lm);
theta(4)=b*Lm/(Ls+Lm) - bm;

```

```

theta(5)=(Ls+Lm)/Lm;
theta(6)=(1+(Lm^2)/(sigma*(Ls+Lm)*(Lr+Lm)))*im0;
theta(7)=b-bm;

% Estimation bounds

rho_theta=50; % parameter error in "percent"
d_theta=abs(theta)*rho_theta/100;
theta_min=theta-d_theta;
theta_max=theta+d_theta;

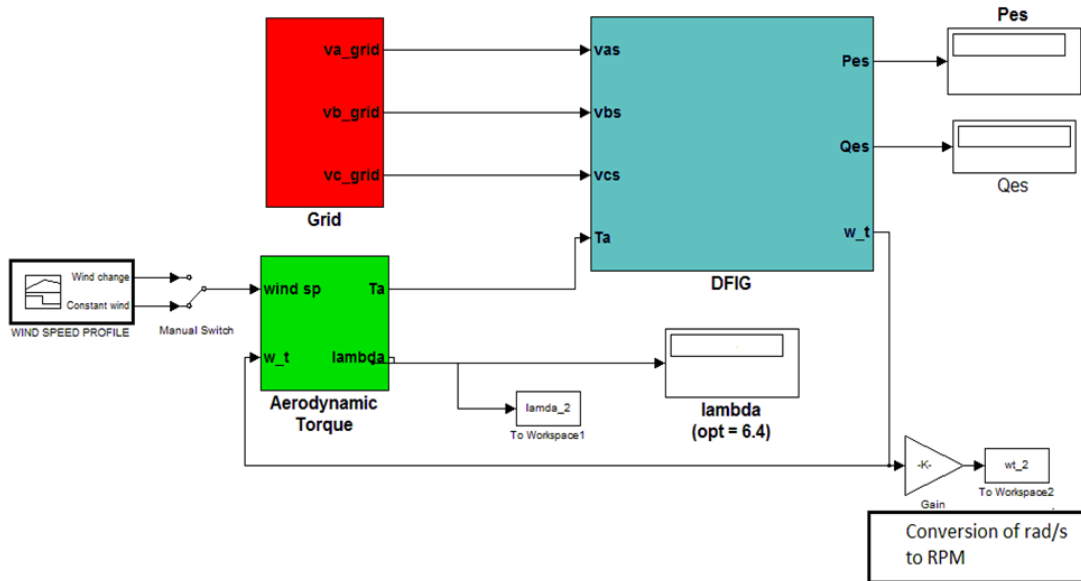
% initial estimates
theta0=theta+d_theta.*(2*rand(1,7)-1);

```

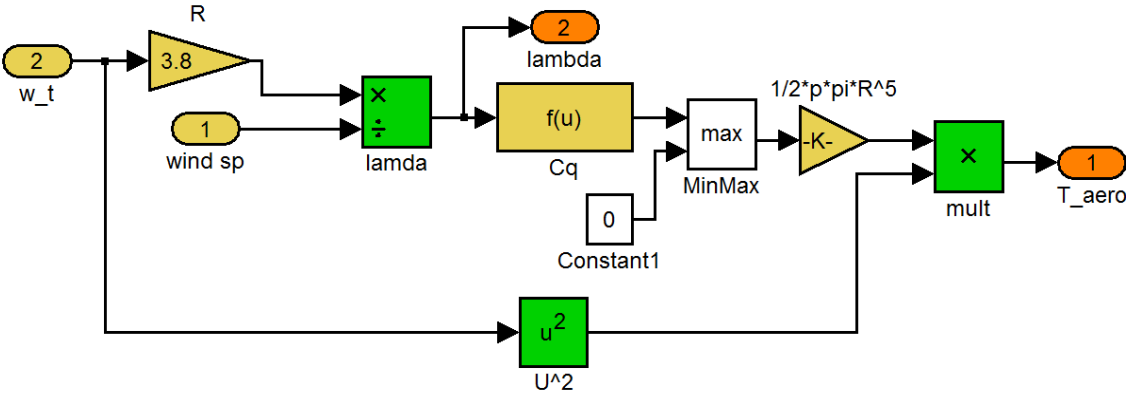
## B. SIMULINK BLOCKS

### 1. First Adaptive Control Approach

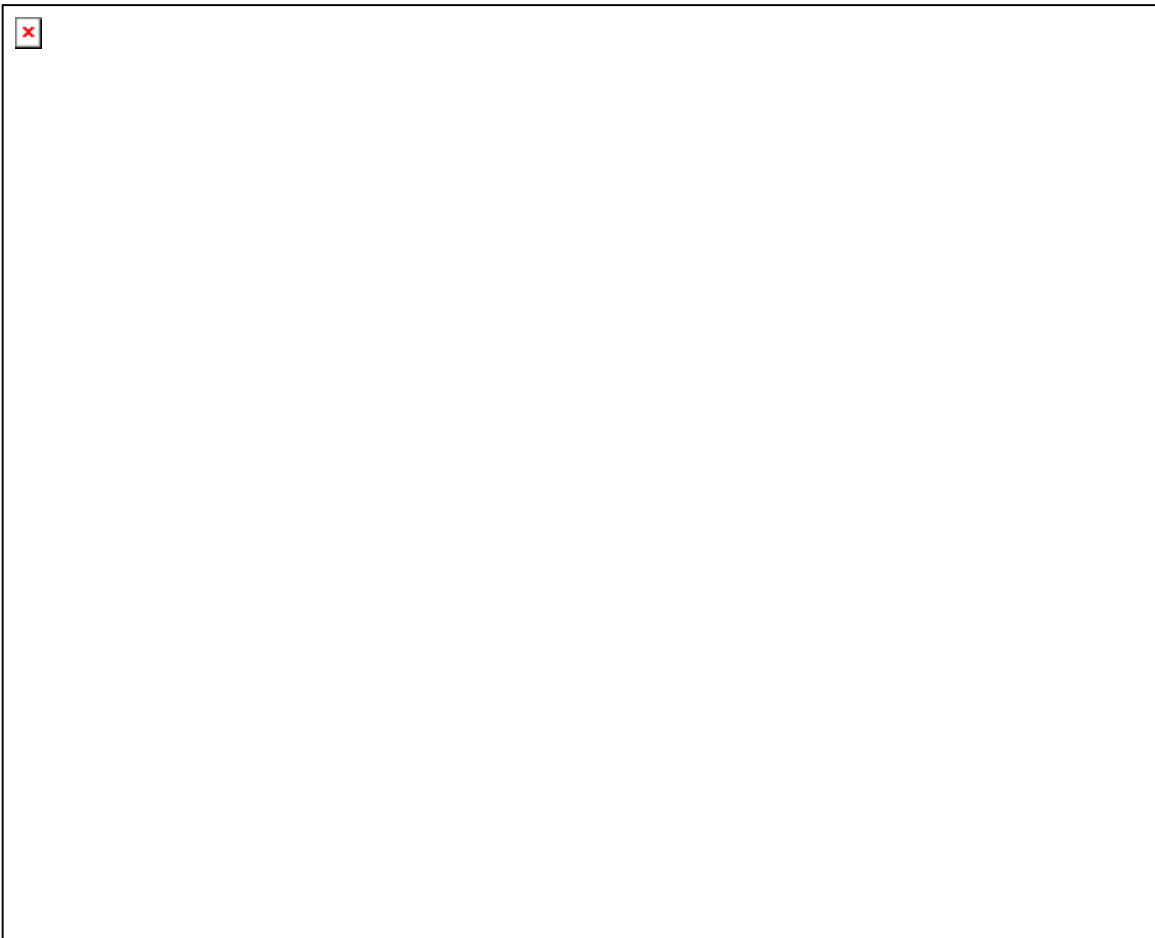
#### a. Overall System View



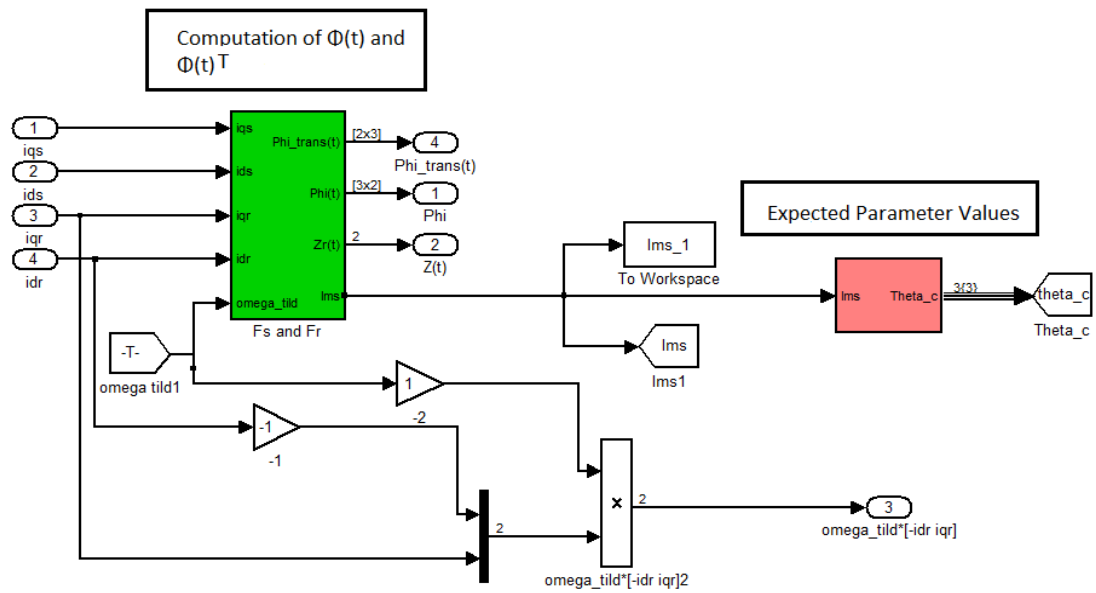
### *b. Aerodynamic Torque Input*



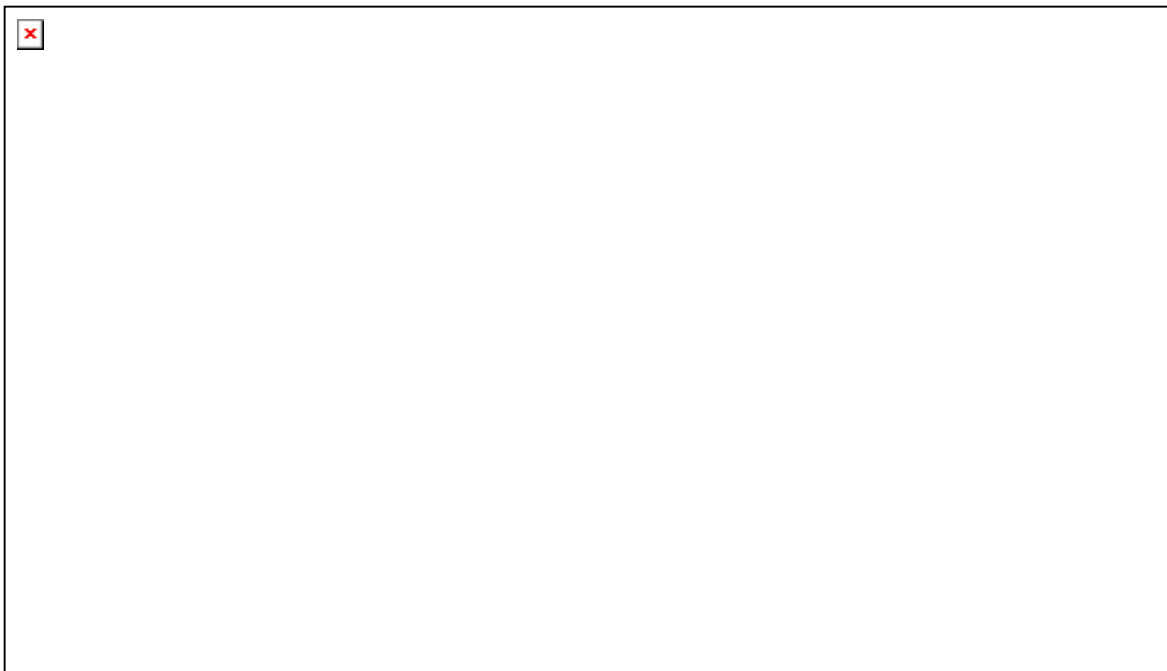
### c. *General View of the Controller*



d. *Preprocess*

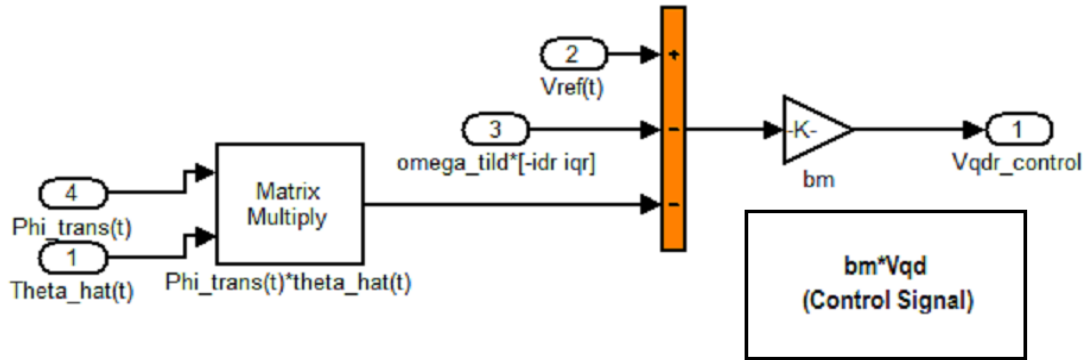


e. *Parameter Estimation*





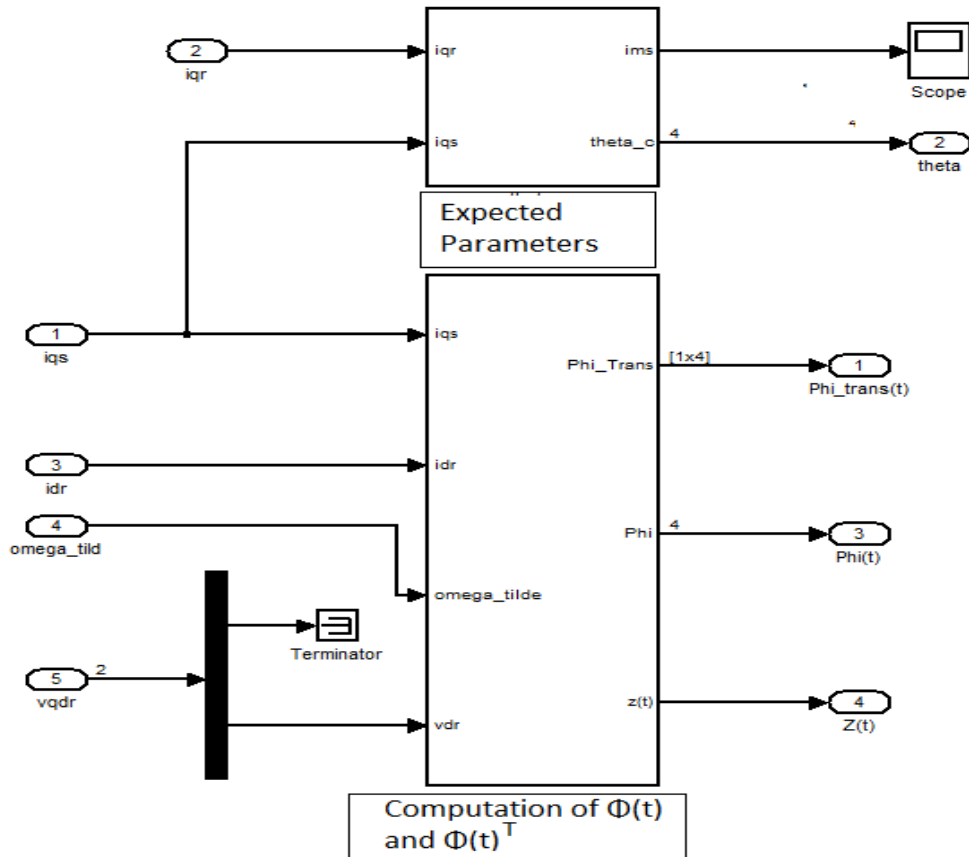
*f. Control*



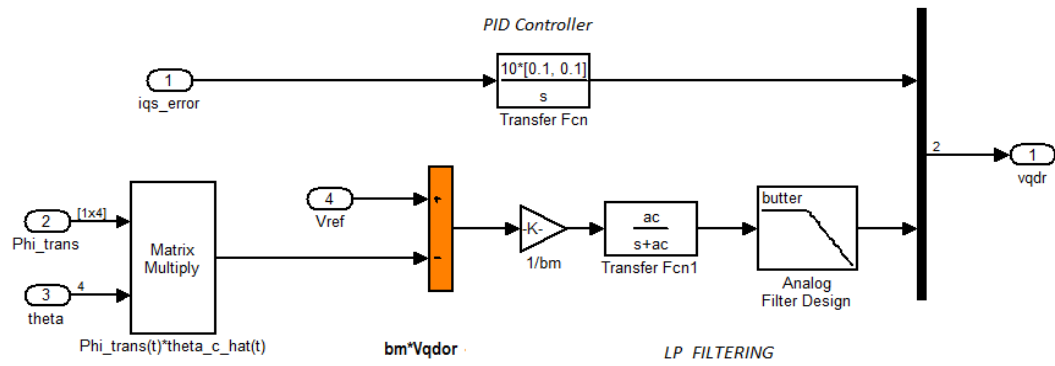
**2. Second Approach**

The above Simulink blocks, in sections *a*, *b*, *c*, *e*, are common for both approaches. Those which are different for the second approach follow.

*a. Preprocess*



## b. Control



THIS PAGE INTENTIONALLY LEFT BLANK

## LIST OF REFERENCES

- [1] U.S. Energy Information Administration (EIA), "International Energy Outlook 2010" [Online]. Available: <http://www.eia.gov/oiaf/ieo/electricity.html> (accessed August 5, 2010).
- [2] F. Birol, "Power to the People, The World Outlook for Electricity Investment," *International Atomic Energy Agency Bulletin*, Bulletin 46/1, pp. 9–12, June 2004.
- [3] REN21, "Renewables 2011 Global Status Report," Technical Report, REN21 Secretariat, Paris, 2011.
- [4] U.S. Department of Energy, Office of Energy Efficiency and Renewable Energy, "20% Wind Energy by 2030," *Technical Report No. DOE/GO-102008-2567*, U.S. DOE, Washington, DC, 2008.
- [5] K. E. Johnson, "Adaptive Torque Control of Variable Speed Wind Turbines," *Technical Report No. NREL/TP-500-36265*, National Renewable Energy Laboratory, Golden, Colorado, August 2004.
- [6] J. I. Jang, Y. S. Kim, and D. C. Lee, "Active and Reactive Power Control of DFIG for Wind Energy Conversion Under Unbalanced Grid Voltage," Presented at Power Electronics and Motion Control Conference, 2006. IPEMC 2006. CES/IEEE 5<sup>th</sup> International, Shanghai, August 2006.
- [7] F. Valenciaga, P. F. Puleston, and S. K. Spurgeon, "A Geometric Approach for the Design of MIMO Sliding Controllers, Application to a Wind-driven Doubly Fed Induction Generator," *Int. J. of Robust and Nonlinear Control*, vol. 19, issue 1, pp. 22–39, January 2009.
- [8] V. Utkin, J. Guldner, and Shi J., *Sliding Mode Control Theory in Electromechanical Systems*, Taylor & Francis, London, 1999.
- [9] A. Sabanovic, L. Fridman, and S. K. Spurgeon, "*Variable Structure Systems: from Principles to Implementation*," IEEE Book Series. IEEE, London, 2004.
- [10] S. A. Frost, M. J. Balas, and A. D. Wright, "Direct Adaptive Control of a Utility-scale Wind Turbine for Speed Regulation," *Int. J. of Robust and Nonlinear Control*, vol. 19, issue 1, pp. 59–71, January 2009.
- [11] A. Martinez, F. Lescher, and J. Y. Zhao, "An Adaptive Control for Wind Turbine," presented, at the International Conference on Renewable Energies and Power Quality 05, Zaragoza, Spain, March 2005.

- [12] R. Pena, J. C. Clare, and G. M. Asher, "Doubly Fed Induction Generator Using Back-to-Back PWM Converters and its Application to Variable Speed Wind-energy Generation," *IEE Proc.-Electr. Power Appl.*, vol. 143, no. 3, pp. 231–241, May 1996.
- [13] S. K. Salman and B. Badrzadeh, "New Approach for Modeling Doubly-Fed Induction Generator (DFIG) for Grid-Connection Studies," presented at 2004 European Wind Energy and Exhibition, London, November 2004.
- [14] F. D. Bianchi, H. De Battista, and R. J. Mantz, *Wind Turbine Control Systems*, pp. 2–28, Springer, London, 2010.
- [15] A. I. Munteanu, A. I. Bratcu, N-A Cutululis, and E. Ceang, *Optimal Control of Wind Energy Systems Towards a Global Approach*, Springer, London, 2008.
- [16] M. O. L. Hansen, *Aerodynamics of Wind Turbines, Second Edition*, Earthscan, London, 2008.
- [17] A. Betz, *Introduction to the Theory of Flow Machines*, Pergamon Press, Oxford, 1966.
- [18] J. F. Manwell, J. G. McGowan, and A. L. Rogers, *Wind Energy Explained: Theory, Design, and Application*, John Wiley and Sons Ltd., West Sussex, England, 2002.
- [19] P. C. Krause, O. Wasynczuk, and S. D. Sudhoff, *Analysis of Electric Machinery and Drive Systems, Second Edition*, John Wiley & Sons, 2002.
- [20] R. De Doncker, D. W. J. Pulle, and A. Veltman, *Advanced Electrical Drives, Analysis, Modelling, Control*, Springer, London, 2011.
- [21] A. L. Julian, Notes for EC4130 (Advanced Electrical Machinery Systems), NPS, 2010 (unpublished).
- [22] P. Ioannou and J. Sun, *Robust Adaptive Control*, Prentice Hall, 1996.
- [23] K. J. Astrom and B. Wittenmark, *Adaptive Control, Second Edition*, Dover Publications, New York, 2008.
- [24] S. Sastry and M. Bodson, *Adaptive Control, Stability, Convergence, and Robustness*, Prentice Hall, New Jersey, 1989.
- [25] J. J. E. Slotline and W. Li, *Applied Nonlinear Control*, Prentice Hall, New Jersey, 1991.

- [26] K. J. Astrom and B. Wittenmark, *Computer Controlled Systems, Theory and Design*, Third Edition, Prentice Hall, New Jersey, 1997.
- [27] R. G. Brown and P. Y.C. Hwang, *Introduction to Random Signals and Applied Kalman Filtering*, Third Edition, Wiley, New York, 1997.
- [28] J. G. Massey, “Doubly Fed Induction Machine Control for Wind Energy Conservation,” M.S. Thesis, NPS, Monterey, CA, 2009.
- [29] J. H. Yang, “Robust Adaptive Control Using a Filtering Action,” PhD dissertation, NPS, Monterey, CA, 2009.
- [30] C. Rohrs, L. Valavani, and M. Athans, and G. Stein, “Robustness of Continuous Time Adaptive Control Algorithms in the Presence of Unmodeled Dynamics,” *IEEE Transactions on Automatic Control*, vol. 30, no. 9, pp. 881–889, September 1985.
- [31] N. Hovakimyan and C. Cao, *LI Adaptive Control Theory*, Society for Industrial and Applied Mathematics, Philadelphia, 2010.
- [32] National Oceanic and Atmospheric Administration, National Weather Service, Definition of Wind Gust. [Online]. Available: <http://www.weather.com/glossary/g.html> (accessed August 9, 2011).
- [33] R. Cristi, Notes for EC4300 (Advanced Topics in Control Systems: Wind Turbine Control), NPS, 2010 (unpublished).

THIS PAGE INTENTIONALLY LEFT BLANK

## INITIAL DISTRIBUTION LIST

1. Defense Technical Information Center  
Ft. Belvoir, Virginia
2. Dudley Knox Library  
Naval Postgraduate School  
Monterey, California
3. Dr. Clark Robertson  
Electrical Engineering and Computer Department  
Code EC/R1  
Naval Postgraduate School  
Monterey, California
4. Dr. Roberto Cristi  
Code EC/C1  
Naval Postgraduate School  
Monterey, California
5. Dr. Alexander Julian  
Electrical Engineering and Computer Department  
Code EC/J1  
Naval Postgraduate School  
Monterey, California
6. Dr. Xiaoping Yun  
Electrical Engineering and Computer Department  
Code EC/Yx  
Naval Postgraduate School  
Monterey, California
7. Embassy of Greece  
Office of Naval Attaché  
Washington, District of Columbia
8. LT Stamatios Orfanos - Pepainas  
Hellenic Navy General Staff  
Athens, Greece